

### 1.9.1.5 Bibliography

- M. L. Bruce and D. L. Pfeil, *Am. Lab.*, 2001, 28.
- *Method 245.7: Mercury in Water by Cold Vapor Atomic Fluorescence Spectrometry*, Revision 2.0. EPA (2005).
- J. D. Winefordner and T. J. Vickers. *Anal. Chem.*, 1964, **36**, 161.

## 1.9.2 Detecting Mercury using Gold Amalgamation and Cold Vapor Atomic Fluorescence Spectroscopy<sup>13</sup>

### 1.9.2.1 Introduction

Mercury poisoning can damage the nervous system, kidneys, and also fetal development in pregnant women, so it is important to evaluate the levels of mercury present in our environment. Some of the more common sources of mercury are in the air (from industrial manufacturing, mining, and burning coal), the soil (deposits, waste), water (byproduct of bacteria, waste), and in food (especially seafood). Although regulation for food, water and air mercury content differs, EPA regulation for mercury content in water is the lowest, and it cannot exceed 2 ppb (27  $\mu\text{g/L}$ ).

In 1972, J. F. Kopp et al. first published a method to detect minute concentrations of mercury in soil, water, and air using gold amalgamation and cold vapor atomic fluorescence spectroscopy. While atomic absorption can also measure mercury concentrations, it is not as sensitive or selective as cold vapour atomic fluorescence spectroscopy (CVAFS).

### 1.9.2.2 Sample preparation

As is common with all forms of atomic fluorescence spectroscopy (AFS) and atomic absorption spectrometry (AES), the sample must be digested, usually with an acid, to break down the compounds so that all the mercury present can be measured. The sample is put in the bubbler with a reducing agent such as stannous chloride ( $\text{SnCl}_2$ ) so that  $\text{Hg}^0$  is the only state present in the sample.

### 1.9.2.3 Gold amalgam and CVAFS

Once the mercury is in its elemental form, the argon enters the bubbler through a gold trap, and carries the mercury vapors out of the bubbler to the first gold trap, after first passing through a soda lime (mixture of  $\text{Ca(OH)}_2$ ,  $\text{NaOH}$ , and  $\text{KOH}$ ) trap where any remaining acid or water vapors are caught. After all the mercury from the sample is absorbed by the first gold trap, it is heated to 450  $^\circ\text{C}$ , which causes the mercury absorbed onto the gold trap to be carried by the argon gas to the second gold trap. Once the mercury from the sample has been absorbed by the second trap, it is heated to 450  $^\circ\text{C}$ , releasing the mercury to be carried by the argon gas into the fluorescence cell, where light at a wavelength of 253.7 nm will be used for mercury samples. The detection limit for mercury using gold amalgamation and CVAFS is around 0.05 ng/L, but the detection limit will vary due to the equipment being used, as well as human error.

### 1.9.2.4 Calculating CVAFS concentrations

A standard solution of mercury should be made, and from this dilutions will be used to make at least five different standard solutions. Depending on the detection limit and what is being analyzed, the concentrations in the standard solutions will vary. Note that what other chemicals the standard solutions contain will depend upon how the sample is digested.

#### Example 1.5

A 1.00 g/mL Hg (1 ppm) working solution is made, and by dilution, five standards are made from the working solution, at 5.0, 10.0, 25.0, 50.0, and 100.0 ng/L (ppt). If these five standards give

<sup>13</sup>This content is available online at <<http://cnx.org/content/m38307/1.1/>>.

peak heights of 10 units, 23 units, 52 units, 110 units, and 207 units, respectively, then (1.79) is used to calculate the calibration factor, where  $CF_x$  is the calibration factor,  $A_x$  is the area of the peak or peak height, and  $C_x$  is the concentration in ng/L of the standard, (1.80).

$$CF_x = A_x/C_x \quad (1.79)$$

$$10/5.0 \text{ ng/L} = 2.00 \text{ units.L/ng} \quad (1.80)$$

The calibration factors for the other four standards are calculated in the same fashion: 2.30, 2.08, 2.20, and 2.07, respectively. The average of the five calibration factors is then taken, (1.81).

$$CF_m = (2.00 + 2.30 + 2.08 + 2.20 + 2.07)/5 = 2.13 \text{ units.L/ng} \quad (1.81)$$

Now to calculate the concentration of mercury in the sample, (1.82) is used, where  $A_s$  is the area of the peak of the sample,  $CF_m$  is the mean calibration factor,  $V_{std}$  is the volume of the standard solution minus the reagents added, and  $V_{smp}$  is the volume of the initial sample (total volume minus volume of reagents added). If  $A_s$  is measured at 49 units,  $V_{std} = 0.47 \text{ L}$ , and  $V_{smp} = 0.26 \text{ L}$ , then the concentration can be calculated, (1.83).

$$[Hg] \text{ (ng/L)} = (A_s/CF_m).(V_{std}/V_{smp}) \quad (1.82)$$

$$(49 \text{ units}/2.13 \text{ units.L/ng}).(0.47 \text{ L}/0.26 \text{ L}) = 43.2 \text{ ng/L of Hg present} \quad (1.83)$$

### 1.9.2.5 Sources of error

Contamination from the sample collection is one of the biggest sources of error: if the sample is not properly collected or hands/gloves are not clean, this can tamper with the concentration. Also, making sure the glassware and equipment is clean from any sources of contamination.

Furthermore, sample vials that are used to store mercury-containing samples should be made out of borosilicate glass or fluoropolymer, because mercury can leach or absorb other materials, which could cause an inaccurate concentration reading.

### 1.9.2.6 Bibliography

- D. L. Pfeil and M. L. Bruce, *Am. Lab.*, 2001, 28.
- *Method 245.7: Mercury in Water by Cold Vapor Atomic Fluorescence Spectrometry*, Revision 2.0. EPA. 2005.
- J. D. Winefordner and T. J. Vickers, *Anal. Chem.*, 1964, **36**, 161.
- *Toxicological profile for mercury*, Agency for Toxic Substances and Disease Registry (ATSDR).
- J. F. Kopp, M. C. Longbottom, and L. B. Lobring, *AWWA*, 1972, **64**, 20.

### 1.9.3 The Application of Fluorescence Spectroscopy in the Mercury Ion Detection<sup>14</sup>

#### 1.9.3.1 Mercury in the environment

Mercury pollution has become a global problem and seriously endangers human health. Inorganic mercury can be easily released into the environment through a variety of anthropogenic sources, such as the coal mining, solid waste incineration, fossil fuel combustion, and chemical manufacturing. It can also be released through the nonanthropogenic sources in the form of forest fires, volcanic emissions, and oceanic emission.

Mercury can be easily transported into the atmosphere as the form of the mercury vapor. The atmospheric deposition of mercury ions leads to the accumulation on plants, in topsoil, in water, and in underwater sediments. Some prokaryotes living in the sediments can convert the inorganic mercury into methylmercury, which can enter food chain and finally is ingested by human.

Mercury seriously endangers people's health. One example is that many people died due to exposure to methylmercury through seafood consumption in Minamata, Japan. Exposure in the organic mercury causes a serious of neurological problems, such as prenatal brain damage, cognitive and motion disorders, vision and hearing loss, and even death. Moreover, inorganic mercury also targets the renal epithelial cells of the kidney, which results in tubular necrosis and proteinuria.

The crisis of mercury in the environment and biological system compel people to carry out related work to confront the challenge. To design and implement new mercury detection tools will ultimately aid these endeavors. Therefore, in this paper, we will mainly introduce fluorescence molecular sensor, which is becoming more and more important in mercury detection due to its easy use, low cost and high efficiency.

#### 1.9.3.2 Introduction of fluorescence molecular sensors

Fluorescence molecular sensor, one type of fluorescence molecular probe, can be fast, reversible response in the recognition process. There are four factors, selectivity, sensitivity, in-situ detection, and real time, that are generally used to evaluate the performance of the sensor. In this paper, four fundamental principles for design fluorescence molecular sensors are introduced.

##### 1.9.3.2.1 Photoinduced electron transfer (PET)

Photoinduced electron transfer is the most popular principle in the design of fluorescence molecular sensors. The characteristic structure of PET sensors includes three parts as shown in Figure 1.53:

- The fluorophore absorbs the light and emits fluorescence signal.
- The receptor selectively interacts with the guest.
- A spacer connects the fluorophore and receptor together to form an integral system and successfully, effectively transfers the recognition information from receptor to fluorophore.

---

<sup>14</sup>This content is available online at <<http://cnx.org/content/m38321/1.1/>>.

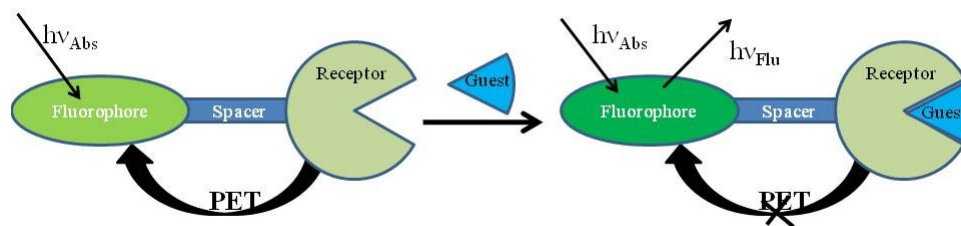


**Figure 1.53:** The general view of the principle of PET fluorescence molecular sensor.

In the PET sensors, photoinduced electron transfer makes the transfer of recognition information to fluorescence signal between receptor and fluorophore come true. Figure 1.53 shows the detailed process of how PET works in the fluorescence molecular sensor. The receptor could provide the electron to the vacated elector orbital of the excited fluorophore. The excited electron in the fluorophore could not come back the original orbital, resulting in the quenching of fluorescence emission. The coordination of receptor and guest decreased the electron donor ability of receptor reduced or even disrupted the PET process, then leading to the enhancement of intensity of fluorescence emission. Therefore, the sensors had weak or no fluorescence emission before the coordination. However, the intensity of fluorescence emission would increase rapidly after the coordination of receptor and guest.

#### 1.9.3.2.2 Intramolecular charge transfer (ICT)

Intramolecular charge transfer (ICT) is also named photoinduced charge transfer. The characteristic structure of ICT sensors includes only the fluorophore and recognition group, but no spacer. The recognition group directly binds to the fluorophore. The electron withdrawing or electron donating substituents on the recognition group plays an important role in the recognition. When the recognition happens, the coordination between the recognition group and guest affects the electron density in the fluorophore, resulting in the change of fluorescence emission in the form of blue shift or red shift.

#### 1.9.3.2.3 Excimer

When the two fluorophores are in the proper distance, an intermolecular excimer can be formed between the excited state and ground state. The fluorescence emission of the excimer is different with the monomer and mainly in the form of new, broad, strong, and long wavelength emission without fine structures. The proper distance determines the formation of excimer, therefore modulation of the distance between the two fluorophores becomes crucial in the design of the sensors based on this mechanism. The fluorophores have long lifetime in the singlet state to be easily forming the excimers. They are often used in such sensors.

#### 1.9.3.2.4 Fluorescence resonance energy transfer (FRET)

FRET is a popular principle in the design of the fluorescence molecular sensor. In one system, there are two different fluorophores, in which one acts as a donor of excited state energy to the receptor of the other. As shown in Figure 1.54, the receptor accepts the energy from the excited state of the donor and gives the fluorescence emission, while the donor will return back to the electronic ground state. There are three factors affecting the performance of FRET. They are the distance between the donor and the acceptor, the proper

orientation between the donor emission dipole moment and acceptor absorption moment, and the extent of spectral overlap between the donor emission and acceptor absorption spectrum (Figure 1.55).

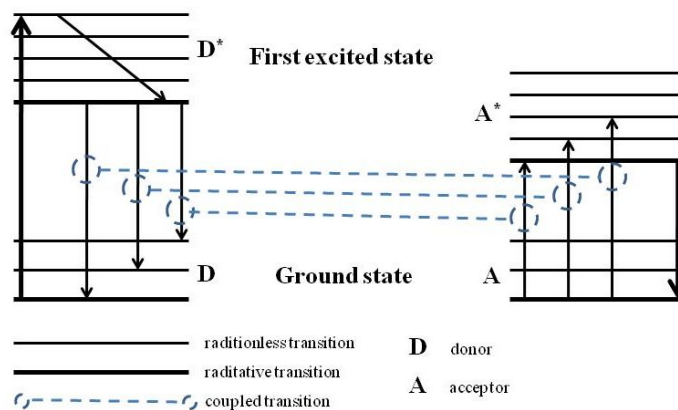


Figure 1.54: A schematic fluorescence resonance energy transfer system.

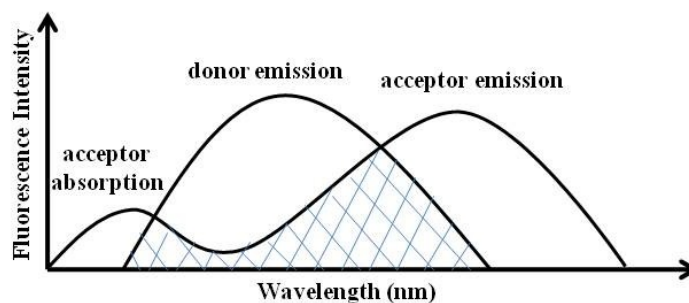


Figure 1.55: Diagram showing the spectral overlap for fluorescence resonance energy transfer system.

### 1.9.3.3 Introduction of fluorescence spectroscopy

#### 1.9.3.3.1 Fluorescence

Fluorescence is a process involving the emission of light from any substance in the excited states. Generally speaking, fluorescence is the emission of electromagnetic radiation (light) by the substance absorbed the different wavelength radiation. Its absorption and emission is illustrated in the Jablonski diagram (Figure 1.56), a fluorophore is excited to higher electronic and vibrational state from ground state after excitation. The

excited molecules can relax to lower vibrational state due to the vibrational relaxation and, then further return to the ground state in the form of fluorescence emission.

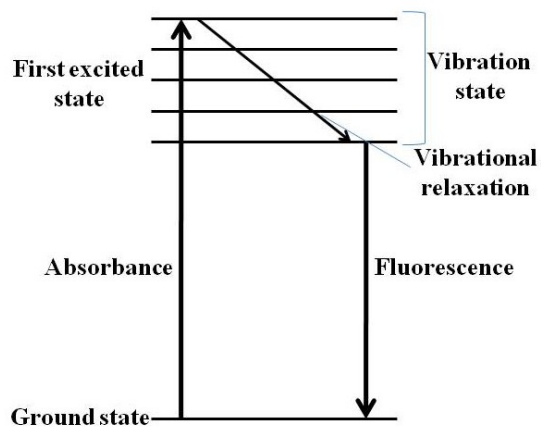


**Figure 1.56:** Jablonski diagram of fluorescence.

---

### 1.9.3.3.2 Instrumentation

Most spectrofluorometers can record both excitation and emission spectra. They mainly consist of four parts: light sources, monochromators, optical filters and detector (Figure 1.57).

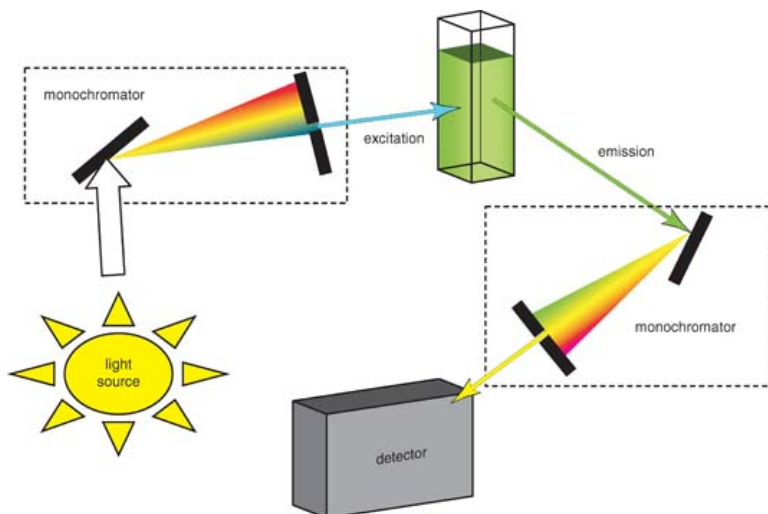


**Figure 1.57:** Schematic representation of a fluorescence spectrometer.

#### 1.9.3.3.2.1 Light sources

Light sources that can emit wavelength of light over the ultraviolet and the visible range can provide the excitation energy. There are different light sources, including arc and incandescent xenon lamps, high-pressure mercury (Hg) lamps, Xe-Hg arc lamps, low pressure Hg and Hg-Ar lamps, pulsed xenon lamps, quartz-tungsten halogen (QTH) lamps, LED light sources, etc. The proper light source is chosen based on the application.

#### 1.9.3.3.2.2 Monochromators

Prisms and diffraction gratings are two mainly used types of monochromators, which help to get the experimentally needed chromatic light with a wavelength range of 10 nm. Typically, the monochromators are evaluated based on dispersion, efficiency, stray light level and resolution.

#### 1.9.3.3.2.3 Optical filters

Optical filters are used in addition to monochromators in order to further purifying the light. There are two kinds of optical filters. The first one is the colored filter, which is the most traditional filter and is also divided into two categories: monochromatic filter and long-pass filter. The other one is thin film filter that is the supplement for the former one in the application and being gradually instead of colored filter.

#### 1.9.3.3.2.4 Detector

An InGaAs array is the standard detector used in many spectrofluorometers. It can provide rapid and robust spectral characterization in the near-IR.

### 1.9.3.4 Applications

#### 1.9.3.4.1 PET fluorescence sensor

As a PET sensor 2-{5-[(2-{[bis-(2-ethylsulfanyl-ethyl)-amino]-methyl}-phenylamino)-methyl]-2-chloro-6-hydroxy-3-oxo-3H-xanthen-9-yl]-benzoic acid (MS1) (Figure 1.58) shows good selectivity for mercury ions in buffer solution (pH = 7, 50 mM PIPES, 100 mM KCl). From Figure 1.59, it is clear that, upon the increase of the concentration of  $\text{Hg}^{2+}$  ions, the coordination between the sensor and  $\text{Hg}^{2+}$  ions disrupted the PET process, leading to the increase of the intensity of fluorescence emission with slight red shift to 528 nm. Sensor MS1 also showed good selectivity for  $\text{Hg}^{2+}$  ions over other cations of interest as shown in the right bars in Figure 1.60; moreover, it had good resistance to the interference from other cations when detected  $\text{Hg}^{2+}$  ions in the mixture solution excluding  $\text{Cu}^{2+}$  ions as shown in the dark bars in the Figure 1.60.

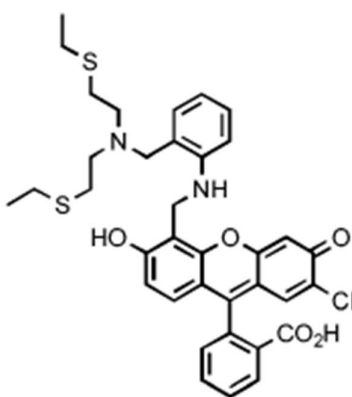


**Figure 1.58:** Structure of the PET fluorescence sensor 2-{5-[(2-{[bis-(2-ethylsulfanyl-ethyl)-amino]-methyl}-phenylamino)-methyl]-2-chloro-6-hydroxy-3-oxo-3H-xanthen-9-yl]-benzoic acid.

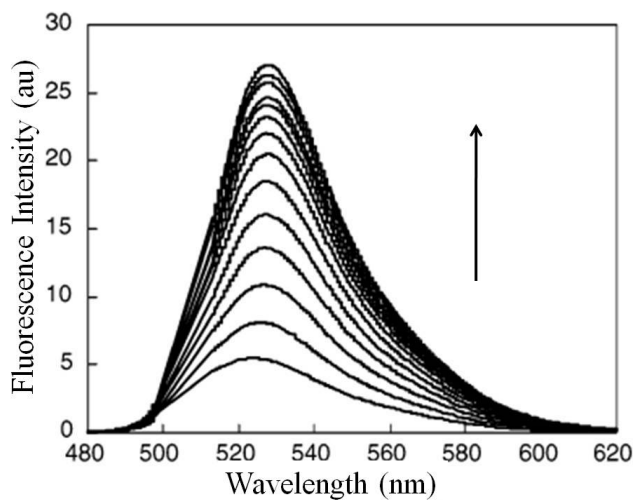


**Figure 1.59:** Fluorescence spectra of sensor MS1 ( $1 \mu\text{M}$ ) upon addition of  $\text{Hg}^{2+}$  ( $0 - 3 \mu\text{M}$ ) in buffer solution ( $\text{pH} = 7$ ,  $50 \text{ mM PIPES}$ ,  $100 \text{ mM KCl}$ ) with an excitation of  $500 \text{ nm}$ .

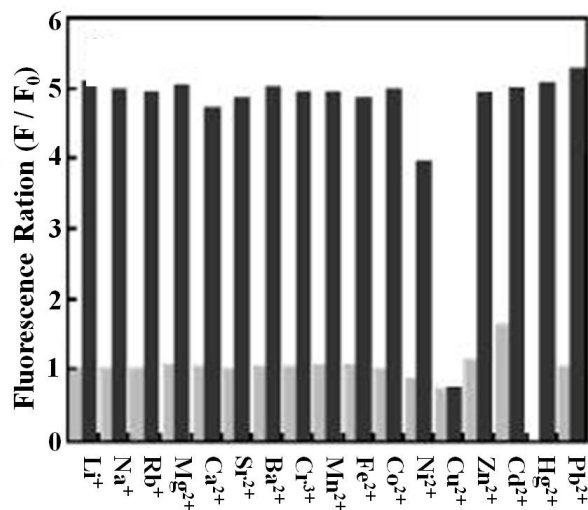


**Figure 1.60:** The selectivity of MS1 for  $\text{Hg}^{2+}$  ions in the presence of other cations of interest. The light bars represent the emission of MS1 in the presence of 67 equiv of the interested cations. The dark bars represent the change in integrated emission that occurs upon subsequent addition of 67 equiv of  $\text{Hg}^{2+}$  to the mixed solution.

### 1.9.3.4.2 ICT fluorescence sensor

2,2',2'',2'''-(3-(benzo[d]thiazol-2-yl)-2-oxo-2-H-chromene-6,7-diyl) *bis*(azanetriyl)tetrakis(N-(2-hydroxyethyl)acetamide) (RMS) (Figure 1.61) has been shown to be an ICT fluorescence sensor. From Figure 1.62, it is clear that, with the gradual increase of the concentration of  $\text{Hg}^{2+}$  ions, fluorescence emission spectra revealed a significant blue shift, which was about 100-nm emission band shift from 567 to 475 nm in the presence of 40 equiv of  $\text{Hg}^{2+}$  ions. The fluorescence change came from the coexistence of two electron-rich aniline nitrogen atoms in the electron-donating receptor moiety, which prevented  $\text{Hg}^{2+}$  ions ejection from them simultaneously in the excited ICT fluorophore. Sensor RMS also showed good selectivity over other cations of interest. As shown in Figure 1.63, it is easy to find that only  $\text{Hg}^{2+}$  ions can modulate the fluorescence of RMS in a neutral buffered water solution.

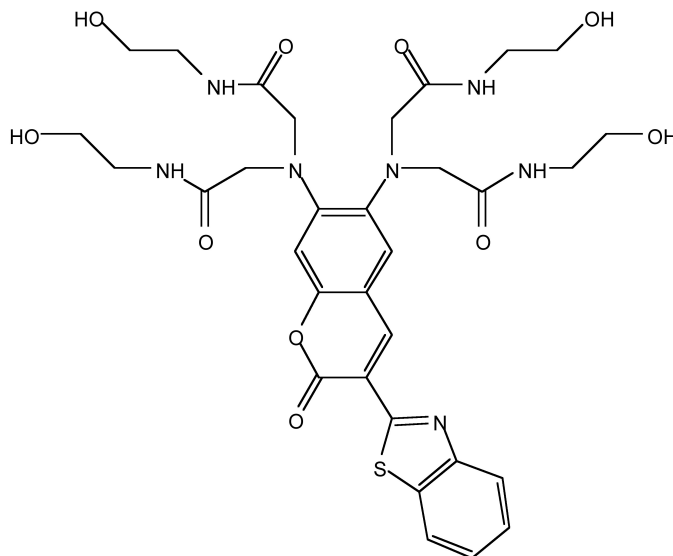


**Figure 1.61:** Structure of the ICT fluorescence sensor 2,2',2'',2'''-(3-(benzo[d]thiazol-2-yl)-2-oxo-2-H-chromene-6,7-diyl) *bis*(azanetriyl) tetrakis(N-(2-hydroxyethyl)acetamide) (RMS).

---

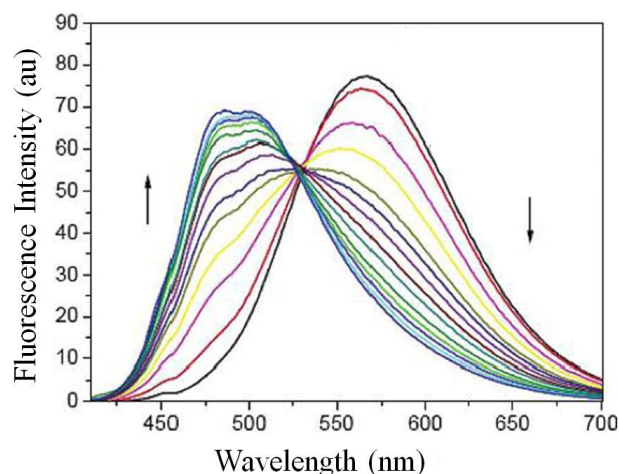


**Figure 1.62:** Fluorescence spectra of RMS ( $5 \mu\text{M}$ ) upon addition of  $\text{Hg}^{2+}$  ( $0 \mu\text{M}$  to  $200 \mu\text{M}$ ) in  $0.05 \text{ M}$  phosphate-buffered water solution (pH 7.5) with an excitation of  $390 \text{ nm}$ .



**Figure 1.63:** Fluorescence response of  $10 \mu\text{M}$  RMS in the presence of 20 equiv of different cations of interest at the same condition: control (0),  $\text{Cd}^{2+}$  (1),  $\text{Hg}^{2+}$  (2),  $\text{Fe}^{3+}$  (3),  $\text{Zn}^{2+}$  (4),  $\text{Ag}^+$  (5),  $\text{Co}^{2+}$  (6),  $\text{Cu}^{2+}$  (7),  $\text{Ni}^{2+}$  (8), and  $\text{Pb}^{2+}$  (9).

#### 1.9.3.4.3 Excimer fluorescence sensor

The (NE,N'E)-2,2'-(ethane-1,2-diyl-bis(oxy))bis(N-(pyren-4-ylmethylene)aniline) (BA) (Figure 1.64) is the excimer fluorescence sensor. As shown in Figure 1.65, when BA existed without mercury ions in the mixture of HEPES- $\text{CH}_3\text{CN}$  (80:20, v/v, pH 7.2), it only had the weak monomer fluorescence emission. Upon the increase of the concentration of mercury ions in the solution of BA, a strong excimer fluorescence emission at  $462 \text{ nm}$  appeared and increased with the change of the concentration of mercury ions. From Figure 1.66, it is clear that BA showed good selectivity for mercury ions. Moreover, it had good resistance to the interference when detecting mercury ions in the mixture solution.

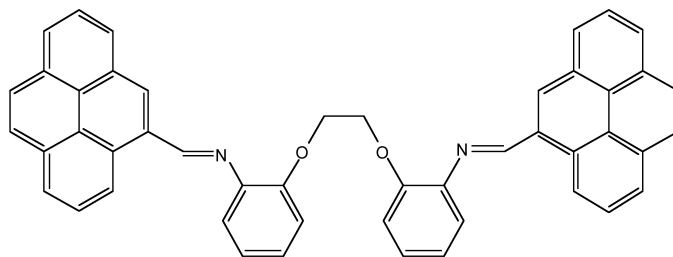


**Figure 1.64:** Structure of the excimer fluorescence sensor (NE,N'E)-2,2'-(ethane-1,2-diyl-bis(oxy)) bis(N-(pyren-4-ylmethylene) aniline) (BA).

---

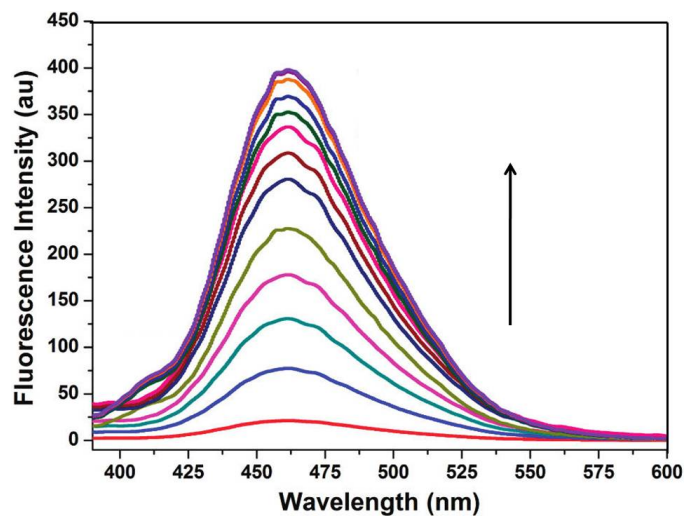


**Figure 1.65:** Fluorescence spectra of BA ( $1 \mu\text{M}$ ) upon addition of  $\text{Hg}^{2+}$  ( $0 \mu\text{M}$  to  $10 \mu\text{M}$ ) in the mixture of HEPES- $\text{CH}_3\text{CN}$  (80:20, v/v, pH 7.2) with an excitation of 365 nm.

---

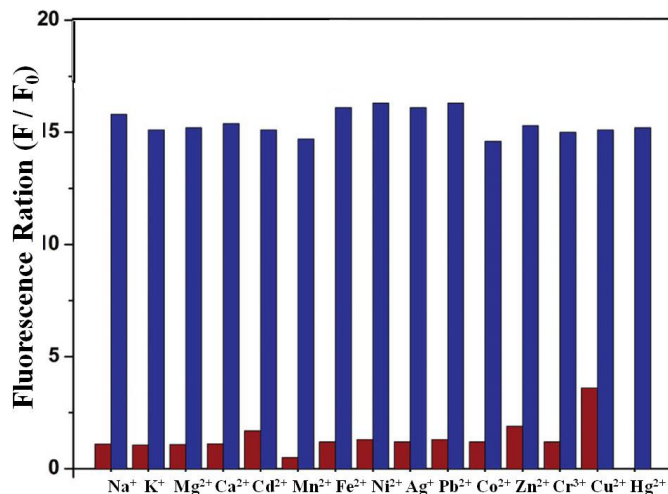


**Figure 1.66:** Fluorescence response of BA ( $1 \mu\text{M}$ ) with 10 equiv of other cations of interest in the same condition. Bars represent the final ( $F$ ) over the initial ( $F_0$ ) integrated emission. The red bars represent the addition of the competing metal ion to a  $1 \mu\text{M}$  solution of BA. The blue bars represent the change of the emission that occurs upon the subsequent addition of  $10 \mu\text{M}$   $\text{Hg}^{2+}$  to the above solution.

#### 1.9.3.4.4 FRET fluorescence sensor

The calix[4]arene derivative bearing two pyrene and rhodamine fluorophores (CPR) (Figure 1.67) is a characteristic FRET fluorescence sensor. Fluorescence titration experiment of CPR ( $10.0 \mu\text{M}$ ) with  $\text{Hg}^{2+}$  ions was carried out in  $\text{CHCl}_3/\text{CH}_3\text{CN}$  (50:50, v/v) with an excitation of 343 nm. As shown in Figure 1.68, upon gradual increase the concentration of  $\text{Hg}^{2+}$  ions in the solution of CPR, the increased fluorescence emission of the ring-opened rhodamine at 576 nm was observed with a concomitantly declining excimer emission of pyrene at 470 nm. Moreover, an isosbestic point centered at 550 nm appeared. This change in the fluorescence emission demonstrated that an energy from the pyrene excimer transferred to rhodamine, resulting from the trigger of  $\text{Hg}^{2+}$  ions. Figure 1.69 showed that CPR had good resistance to other cations of interest when detected  $\text{Hg}^{2+}$  ions, though  $\text{Pb}^{2+}$  ions had little interference in this process.



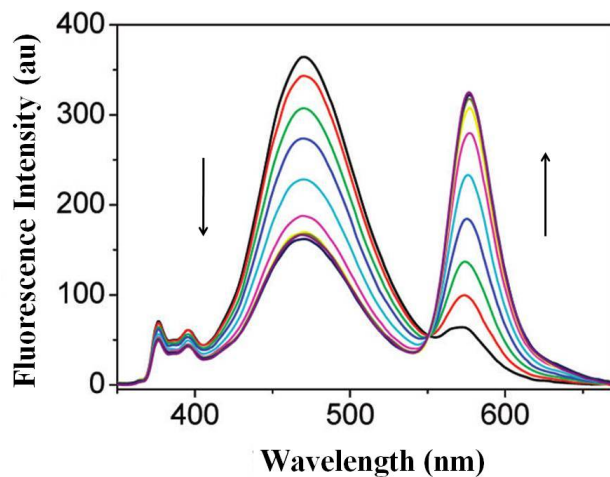


**Figure 1.68:** Fluorescence spectra of CPR (10.0  $\mu\text{M}$ ) in  $\text{CHCl}_3/\text{CH}_3\text{CN}$  (50:50, v/v) upon addition of different concentrations of  $\text{Hg}(\text{ClO}_4)_2$  (0  $\mu\text{M}$  to 30  $\mu\text{M}$ ).

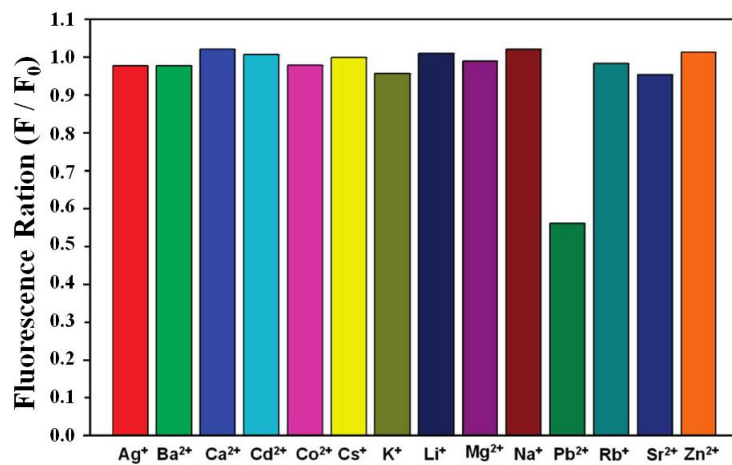


**Figure 1.69:** Competition experiment of 10.0  $\mu\text{M}$  CPR at 576 nm with 10 equiv of other cations of interest in the presence of  $\text{Hg}^{2+}$  (3 equiv) in the same condition.  $F_0$  and  $F$  denote the fluorescence intensity of CPR and  $\text{Hg}^{2+}$  ions and the interested metal ions in the presence of CPR and  $\text{Hg}^{2+}$  ions.

### 1.9.3.5 Bibliography

- E. M. Nolan and S. J. Lippard, *Chem. Rev.*, 2008, **108**, 3443.
- J. S. Kim and D. T. Quang, *Chem. Rev.*, 2007, **107**, 3780.
- E. M. Nolan and S. J. Lippard, *J. Am. Chem. Soc.*, 2003, **125**, 14270.
- J. B. Wang, X. H. Qian, and J. G. Cui, *J. Org. Chem.*, 2006, **71**, 4308.
- Y. H. Lee, M. H. Lee, J. F. Zhang, and J. S. Kim, *J. Org. Chem.*, 2010, **75**, 7159.
- Y. Zhou, C. Y. Zhu, X. S. Gao, X. Y. You, and C. Yao, *Org. Lett.*, 2010, **12**, 2566.
- J. R. Lakowicz, *Principles of Fluorescence Spectroscopy*, 3<sup>rd</sup> Edition, Springer (2006).

## 1.10 An Introduction to Energy Dispersive X-ray Spectroscopy<sup>15</sup>

### 1.10.1 Introduction

Energy-dispersive X-ray spectroscopy (EDX or EDS) is an analytical technique used to probe the composition of a solid materials. Several variants exist, but the all rely on exciting electrons near the nucleus, causing more distant electrons to drop energy levels to fill the resulting “holes.” Each element emits a different set of X-ray frequencies as their vacated lower energy states are refilled, so measuring these emissions can provide both qualitative and quantitative information about the near-surface makeup of the sample. However, accurate interpretation of this data is dependent on the presence of high-quality standards, and technical limitations can compromise the resolution.

### 1.10.2 Physical underpinnings

In the quantum mechanical model of the atom, an electron’s energy state is defined by a set of quantum numbers. The primary quantum number,  $n$ , provides the coarsest description of the electron’s energy level, and all the sublevels that share the same primary quantum number are sometimes said to comprise an energy “shell.” Instead of describing the lowest-energy shell as the “ $n = 1$  shell,” it is more common in spectroscopy to use alphabetical labels: The K shell has  $n = 1$ , the L shell has  $n = 2$ , the M shell has  $n = 3$ , and so on. Subsequent quantum numbers divide the shells into subshells: one for K, three for L, and five for M. Increasing primary quantum numbers correspond with increasing average distance from the nucleus and increasing energy (Figure 1.70). An atom’s core shells are those with lower primary quantum numbers than the highest occupied shell, or valence shell.

---

<sup>15</sup>This content is available online at <<http://cnx.org/content/m43555/1.1/>>.

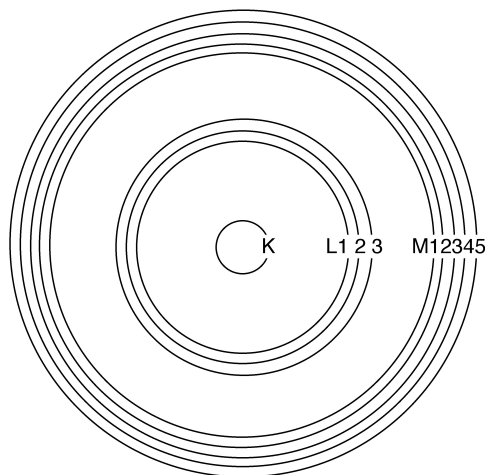


**Figure 1.70:** A diagram of the core electronic energy levels of an atom, with the lowest energy shell, K, nearest the nucleus. Circles are used here for convenience – they are not meant to represent the shapes of the electron’s orbitals. Adapted from *Introduction to Energy Dispersive X-ray Spectroscopy (EDS)*, <http://micron.ucr.edu/public/manuals/EDS-intro.pdf><sup>16</sup>.

---

Transitions between energy levels follow the law of conservation of energy. Excitation of an electron to a higher energy state requires an input of energy from the surroundings, and relaxation to a lower energy state releases energy to the surroundings. One of the most common and useful ways energy can be transferred into and out of an atom is by electromagnetic radiation. Core shell transitions correspond to radiation in the X-ray portion of the spectrum; however, because the core shells are normally full by definition, these transitions are not usually observed.

X-ray spectroscopy uses a beam of electrons or high-energy radiation (see instrument variations, below) to excite core electrons to high energy states, creating a low-energy vacancy in the atoms’ electronic structures. This leads to a cascade of electrons from higher energy levels until the atom regains a minimum-energy state. Due to conservation of energy, the electrons emit X-rays as they transition to lower energy states. It is these X-rays that are being measured in X-ray spectroscopy. The energy transitions are named using the letter of the shell where ionization first occurred, a Greek letter denoting the group of lines that transition belongs to, in order of decreasing importance, and a numeric subscript ranking the peak’s intensity within that group. Thus, the most intense peak resulting from ionization in the K shell would be  $K\alpha_1$  (Figure 1.71). Since each element has a different nuclear charge, the energies of the core shells and, more importantly, the spacing between them vary from one element to the next. While not every peak in an element’s spectrum is exclusive to that element, there are enough characteristic peaks to be able to determine composition of the sample, given sufficient resolving power.

<sup>16</sup><http://micron.ucr.edu/public/manuals/EDS-intro.pdf>

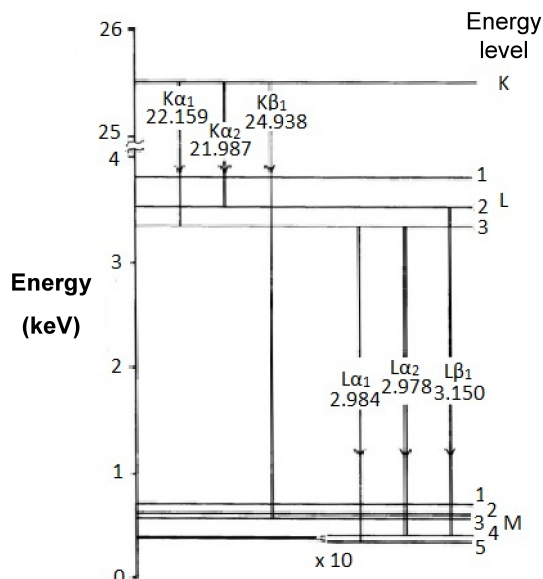


**Figure 1.71:** A diagram of the energy transitions after the excitation of a gold atom. The arrows show the direction the vacancy moves when the higher energy electrons move down to refill the core. Adapted from *Introduction to Energy Dispersive X-ray Spectroscopy (EDS)*, <http://micron.ucr.edu/public/manuals/EDS-intro.pdf><sup>17</sup>.

### 1.10.3 Instrumentation and sample preparation

#### 1.10.3.1 Instrument variations

There are two common methods for exciting the core electrons off the surface atoms. The first is to use a high-energy electron beam like the one in a scanning electron microscope (SEM). The beam is produced by an electron gun, in which electrons emitted thermionically from a hot cathode are guided down the column by an electric field and focused by a series of negatively charged “lenses.” X-rays emitted by the sample strike a lithium-drifted silicon *p-i-n* junction plate. This promotes electrons in the plate into the conduction band, inducing a voltage proportional to the energy of the impacting X-ray which generally falls between about 1 and 10 keV. The detector is cooled to liquid nitrogen temperatures to reduce electronic noise from thermal excitations.

It is also possible to use X-rays to excite the core electrons to the point of ionization. In this variation, known as energy-dispersive X-ray fluorescence analysis (EDXRFA or XRF), the electron column is replaced by an X-ray tube and the X-rays emitted by the sample in response to the bombardment are called secondary X-rays, but these variants are otherwise identical.

Regardless of the excitation method, subsequent interactions between the emitted X-rays and the sample can lead to poor resolution in the X-ray spectrum, producing a Gaussian-like curve instead of a sharp peak. Indeed, this spreading of energy within the sample combined with the penetration of the electron or X-ray beam leads to the analysis of a roughly  $1 \mu\text{m}^3$  volume instead of only the surface features. Peak broadening can lead to overlapping peaks and a generally misleading spectrum. In cases where a normal EDS spectrum

<sup>17</sup><http://micron.ucr.edu/public/manuals/EDS-intro.pdf>

is inadequately resolved, a technique called wavelength-dispersive X-ray spectroscopy (WDS) can be used. The required instrument is very similar to the ones discussed above, and can use either excitation method. The major difference is that instead of having the X-rays emitted by the sample hit the detector directly, they first encounter an analytical crystal of known lattice dimensions. Bragg's law predicts that the strongest reflections off the crystal will occur for wavelengths such that the path difference between rays reflecting from consecutive layers in the lattice is equal to an integral number of wavelengths. This is represented mathematically as (1.84), where  $n$  is an integer,  $\lambda$  is the wavelength of impinging light,  $d$  is the distance between layers in the lattice, and  $\theta$  is the angle of incidence. The relevant variables for the equation are labeled in Figure 1.72.

$$n\lambda = 2d \sin\theta \quad (1.84)$$

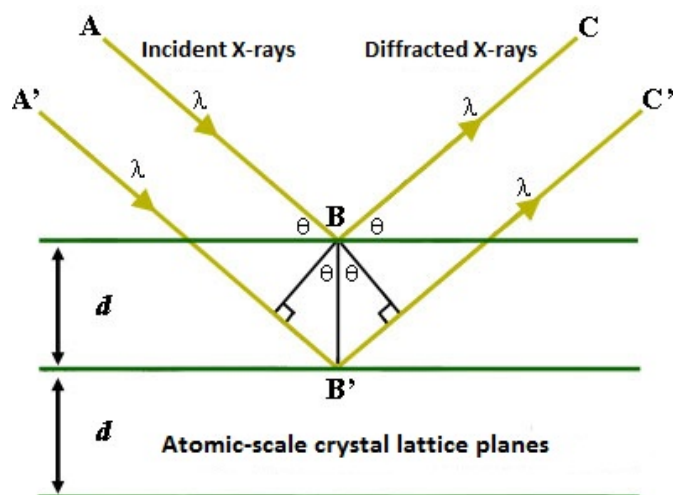


**Figure 1.72:** A diagram of a light beam impinging on a crystal lattice. If the light meets the criterion  $n\lambda = 2d \sin(\theta)$ , Bragg's law predicts that the waves reflecting off each layer of the lattice interfere constructively, leading to a strong signal. Adapted from D. Henry, N. Eby, J. Goodge, and D. Mogk, *X-ray Reflection in Accordance with Bragg's Law*, [http://serc.carleton.edu/research\\_education/geochemsheets/BraggsLaw.html](http://serc.carleton.edu/research_education/geochemsheets/BraggsLaw.html)<sup>18</sup>.

By moving the crystal and the detector around the Rowland circle, the spectrometer can be tuned to examine specific wavelengths (Figure 1.73). Generally, an initial scan across all wavelengths is taken first, and then the instrument is programmed to more closely examine the wavelengths that produced strong peaks. The resolution available with WDS is about an order of magnitude better than with EDS because the analytical crystal helps filter out the noise of subsequent, non-characteristic interactions. For clarity, "X-ray spectroscopy" will be used to refer to all of the technical variants just discussed, and points made about EDS will hold true for XRF unless otherwise noted.

<sup>18</sup>[http://serc.carleton.edu/research\\_education/geochemsheets/BraggsLaw.html](http://serc.carleton.edu/research_education/geochemsheets/BraggsLaw.html)

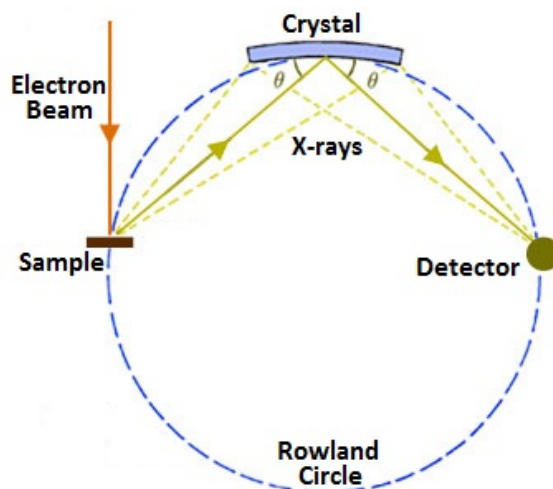


**Figure 1.73:** A schematic of a typical WDS instrument. The analytical crystal and the detector can be moved around an arc known as the Rowland Circle. This grants the operator the ability to change the angle between the sample, the crystal, and the detector, thereby changing the X-ray wavelength that would satisfy Bragg's law. The sample holder is typically stationary. Adapted from D. Henry and J. Goodge, *Wavelength-Dispersive X-ray Spectroscopy (WDS)*, [http://serc.carleton.edu/research\\_education/geochemsheets/wds.html](http://serc.carleton.edu/research_education/geochemsheets/wds.html)<sup>19</sup>.

### 1.10.3.2 Sample preparation

Compared with some analytical techniques, the sample preparation required for X-ray spectroscopy or any of the related methods just discussed is trivial. The sample must be stable under vacuum, since the sample chamber is evacuated to prevent the atmosphere from interfering with the electron beam or X-rays. It is also advisable to have the surface as clean as possible; X-ray spectroscopy is a near-surface technique, so it should analyze the desired material for the most part regardless, but any grime on the surface will throw off the composition calculations. Simple qualitative readings can be obtained from a solid of any thickness, as long as it fits in the machine, but for reliable quantitative measurements, the sample should be shaved as thin as possible.

### 1.10.4 Data interpretation

Qualitative analysis, the determination of which elements are present in the sample but not necessarily the stoichiometry, relies on empirical standards. The energies of the commonly used core shell transitions have been tabulated for all the natural elements. Since combinations of elements can act differently than a single element alone, standards with compositions as similar as possible to the suspected makeup of the sample are also employed. To determine the sample's composition, the peaks in the spectrum are matched with peaks from the literature or standards.

Quantitative analysis, the determination of the sample's stoichiometry, needs high resolution to be good enough that the ratio of the number of counts at each characteristic frequency gives the ratio of those elements in the sample. It takes about 40,000 counts for the spectrum to attain a  $2\sigma$  precision of  $\pm 1\%$ . It is important

<sup>19</sup>[http://serc.carleton.edu/research\\_education/geochemsheets/wds.html](http://serc.carleton.edu/research_education/geochemsheets/wds.html)

to note, however, that this is not necessarily the same as the empirical formula, since not all elements are visible. Spectrometers with a beryllium window between the sample and the detector typically cannot detect anything lighter than sodium. Spectrometers equipped with polymer based windows can quantify elements heavier than beryllium. Either way, hydrogen cannot be observed by X-ray spectroscopy.

X-ray spectra are presented with energy in keV on the x-axis and the number of counts on the y-axis. The EDX spectra of biotite and NIST glass K309 are shown as examples (Figure 1.74 and Figure 1.75, respectively). Biotite is a mineral similar to mica which has the approximate chemical formula  $K(Mg,Fe)_3AlSi_3O_{10}(F,OH)_2$ . Strong peaks for manganese, aluminum, silicon, potassium, and iron can be seen in the spectrum. The lack of visible hydrogen is expected, and the absence of oxygen and fluorine peaks suggests the instrument had a beryllium window. The titanium peak is small and unexpected, so it may only be present in trace amounts. K309 is a mix of glass developed by the National Institute for Standards and Technology. The spectrum shows that it contains significant amounts of silicon, aluminum, calcium, oxygen, iron, and barium. The large peak at the far left is the carbon signal from the carbon substrate the glass was placed on.

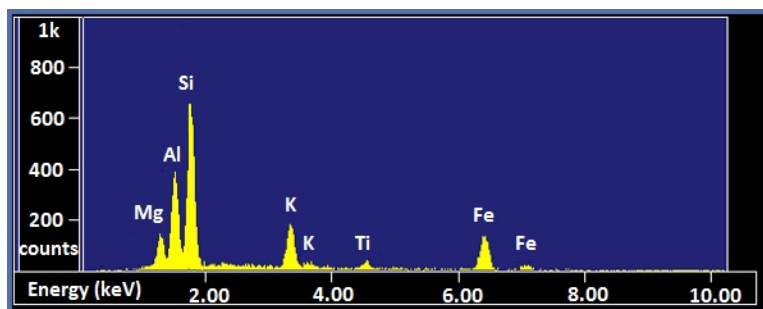


**Figure 1.74:** EDS spectrum of biotite. Silicon, aluminum, manganese, potassium, magnesium, iron, and titanium are all identifiable, though titanium appears to be only a trace component. Adapted from J. Goodge, *Energy-Dispersive X-ray Spectroscopy (EDS)*, [http://serc.carleton.edu/research\\_education/geochemsheets/eds.html](http://serc.carleton.edu/research_education/geochemsheets/eds.html)<sup>20</sup>.

<sup>20</sup>[http://serc.carleton.edu/research\\_education/geochemsheets/eds.html](http://serc.carleton.edu/research_education/geochemsheets/eds.html)

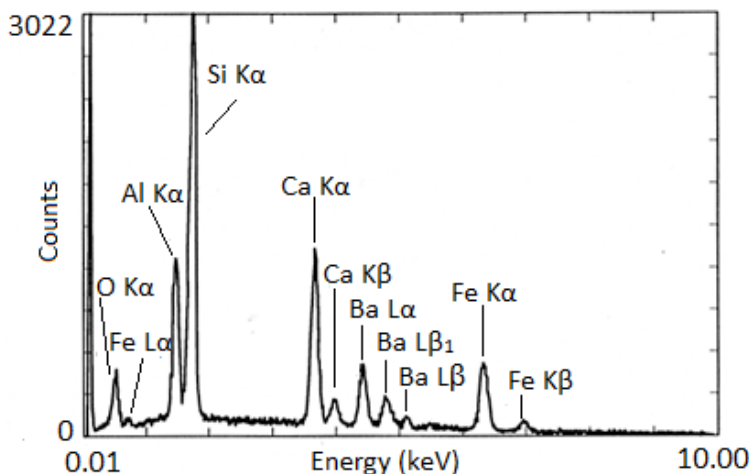


**Figure 1.75:** EDS spectrum of NIST K309 glass. Silicon, aluminum, barium, calcium, iron, and oxygen are identifiable in the spectrum. Adapted from J. Goldstein, D. Newbury, D. Joy, C. Lyman, P. Echlin, E. Lifshin, L. Sawyer, and J. Michael, *Scanning Electron Microscopy and X-ray Microanalysis*, 3<sup>rd</sup>, Springer, New York (2003).

### 1.10.5 Limitations

As has just been discussed, X-ray spectroscopy is incapable of seeing elements lighter than boron. This is a problem given the abundance of hydrogen in natural and man-made materials. The related techniques X-ray photoelectron spectroscopy (XPS) and Auger spectroscopy are able to detect Li and Be, but are likewise unable to measure hydrogen.

X-ray spectroscopy relies heavily on standards for peak identification. Because a combination of elements can have noticeably different properties from the individual constituent elements in terms of X-ray fluorescence or absorption, it is important to use a standard as compositionally similar to the sample as possible. Naturally, this is more difficult to accomplish when examining new materials, and there is always a risk of the structure of the sample being appreciably different than expected.

The energy-dispersive variants of X-ray spectroscopy sometimes have a hard time distinguishing between emissions that are very near each other in energy or distinguishing peaks from trace elements from background noise. Fortunately, the wavelength-dispersive variants are much better at both of these. The rough, stepwise curve in Figure 1.76 represents the EDS spectrum of molybdenite, a mineral with the chemical formula MoS<sub>2</sub>. Broadened peaks make it difficult to distinguish the molybdenum signals from the sulfur ones. Because WDS can select specific wavelengths, it has much better resolution and can pinpoint the separate peaks more accurately. Similarly, the trace silicon signal in the EDS spectrum of the nickel-aluminum-manganese alloy in Figure 1.77A is barely distinguishable as a bump in the baseline, but the WDS spectrum in Figure 1.77B clearly picks it up.

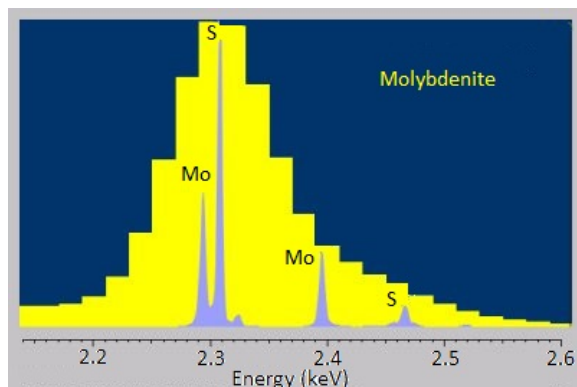


**Figure 1.76:** A comparison of the EDS (yellow) and WDS spectra (light blue) of a sample of molybdenite. The sulfur and molybdenum peaks are unresolved in the EDS spectrum, but are sharp and distinct in the WDS spectrum. Adapted from Oxford Instruments, *The power of WDS sensitivity and resolution*, <http://www.x-raymicroanalysis.com/x-ray-microanalysis-explained/pages/detectors/wave1.htm><sup>21</sup>.

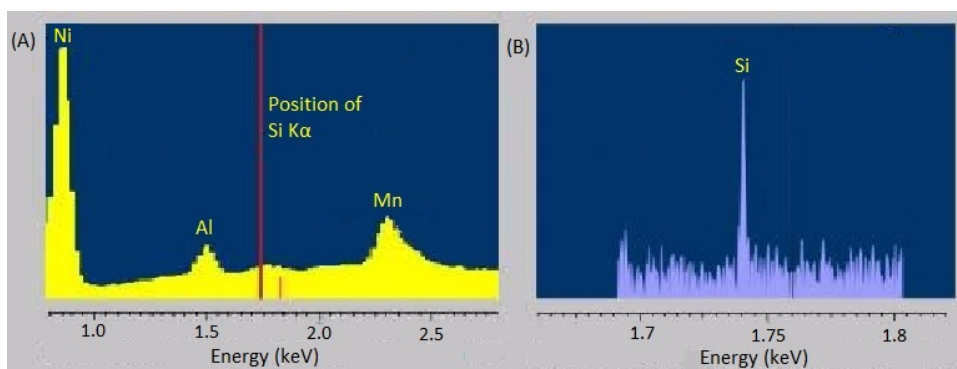


**Figure 1.77:** (A) The EDS spectrum of an alloy comprised primarily of sodium, aluminum, and manganese. Silicon is a trace element in the alloy, but is not discernible in the spectrum. (B) The WDS spectrum of the same alloy in the region around the characteristic silicon peak. In this measurement, the silicon emission stands out quite clearly. Adapted from Oxford Instruments, *The power of WDS sensitivity and resolution*, <http://www.x-raymicroanalysis.com/x-ray-microanalysis-explained/pages/detectors/wave1.htm><sup>22</sup>.

### 1.10.6 Bibliography

- N. A. Baily and G. Kramer, *Radiat. Res.*, 1964, **22**, 53.

<sup>21</sup><http://www.x-raymicroanalysis.com/x-ray-microanalysis-explained/pages/detectors/wave1.htm>

<sup>22</sup><http://www.x-raymicroanalysis.com/x-ray-microanalysis-explained/pages/detectors/wave1.htm>

- J. Goldstein, D. Newbury, D. Joy, C. Lyman, P. Echlin, E. Lifshin, L. Sawyer, and J. Michael, *Scanning Electron Microscopy and X-ray Microanalysis*, 3<sup>rd</sup>, Springer, New York (2003).
- J. Goodge, *Energy-Dispersive X-ray Spectroscopy (EDS)*, [http://serc.carleton.edu/research\\_education/geochemsheets/](http://serc.carleton.edu/research_education/geochemsheets/).
- K. F. J. Heinrich, *Electron Beam Microanalysis*, Van Nostrand Reinhold, New York (1981).
- D. Henry and J. Goodge, *Wavelength-Dispersive X-ray Spectroscopy (WDS)*, [http://serc.carleton.edu/research\\_education/geochemsheets/wds.html](http://serc.carleton.edu/research_education/geochemsheets/wds.html)<sup>24</sup>.
- D. Henry, N. Eby, J. Goodge, and D. Mogk, *X-ray Reflection in Accordance with Bragg's Law*, [http://serc.carleton.edu/research\\_education/geochemsheets/BraggsLaw.html](http://serc.carleton.edu/research_education/geochemsheets/BraggsLaw.html)<sup>25</sup>.
- Oxford Instruments, *The power of WDS sensitivity and resolution*, <http://www.x-raymicroanalysis.com/x-ray-microanalysis-explained/pages/detectors/wavel.htm><sup>26</sup>.
- C. Whiston, *X-ray Methods*, Published on behalf of ACOL, Thames Polytechnic, London, by Wiley, New York (1987).
- S. Zhang, L. Li, and A. Kumar, *Materials Characterisation Techniques*, CRC, Boca Raton (2009).
- *Introduction to Energy Dispersive X-ray Spectroscopy (EDS)*, <http://micron.ucr.edu/public/manuals/EDS-intro.pdf><sup>27</sup>.

## 1.11 X-ray Photoelectron Spectroscopy

### 1.11.1 XPS Analysis of Modified Surfaces<sup>28</sup>

#### 1.11.1.1 Introduction

X-Ray photoelectron spectroscopy (XPS), also known as electron spectroscopy for chemical analysis (ESCA), is one of the most widely used surface techniques in materials science and chemistry. It allows the determination of atomic composition of the sample in a non-destructive manner, as well as other chemical information, such as binding constants, oxidation states and speciation. The sample under study is subjected to irradiation by a high energy X-ray source. The X-rays penetrate only 5 – 20 Å into the sample, allowing for surface specific, rather than bulk chemical, analysis. As an atom absorbs the X-rays, the energy of the X-ray will cause a K-shell electron to be ejected, as illustrated by Figure 1.78. The K-shell is the lowest energy shell of the atom. The ejected electron has a kinetic energy (KE) that is related to the energy of the incident beam ( $h\nu$ ), the electron binding energy (BE), and the work function of the spectrometer ( $\phi$ ) ((1.85)). Thus, the binding energy of the electron can be calculated.

<sup>23</sup>[http://serc.carleton.edu/research\\_education/geochemsheets/eds.html](http://serc.carleton.edu/research_education/geochemsheets/eds.html)

<sup>24</sup>[http://serc.carleton.edu/research\\_education/geochemsheets/wds.html](http://serc.carleton.edu/research_education/geochemsheets/wds.html)

<sup>25</sup>[http://serc.carleton.edu/research\\_education/geochemsheets/BraggsLaw.html](http://serc.carleton.edu/research_education/geochemsheets/BraggsLaw.html)

<sup>26</sup><http://www.x-raymicroanalysis.com/x-ray-microanalysis-explained/pages/detectors/wavel.htm>

<sup>27</sup><http://micron.ucr.edu/public/manuals/EDS-intro.pdf>

<sup>28</sup>This content is available online at <<http://cnx.org/content/m34527/1.1/>>.

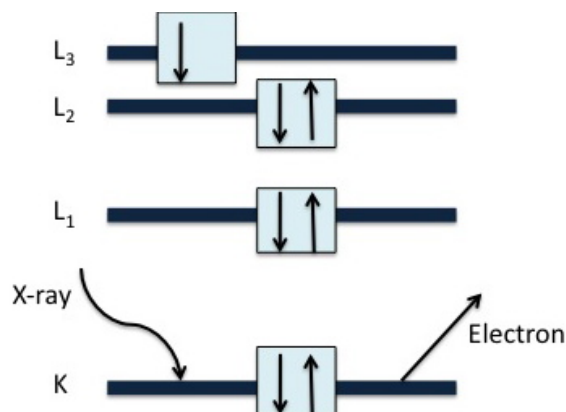


**Figure 1.78:** Excitation of an electron from an atom's K-shell.

$$BE = hv - KE - \phi_s \quad (1.85)$$

Table 1.8 shows the binding energy of the ejected electron, and the orbital from which the electron is ejected, which is characteristic of each element. The number of electrons detected with a specific binding energy is proportional to the number of corresponding atoms in the sample. This then provides the percent of each atom in the sample.

| Element                         | Binding energy (eV) |
|---------------------------------|---------------------|
| Carbon (C) (1s)                 | 284.5 - 285.1       |
| Nitrogen (N) (1s)               | 396.1 - 400.5       |
| Oxygen (O) (1s)                 | 526.2 - 533.5       |
| Silicon (Si) (2p)               | 98.8 - 99.5         |
| Sulfur (S) (2p <sub>3/2</sub> ) | 164.0 - 164.3       |
| Iron (Fe) (2p <sub>3/2</sub> )  | 706.8 - 707.2       |
| Gold (Au) (4f <sub>7/2</sub> )  | 83.8 - 84.2         |

**Table 1.8:** Binding energies for select elements in their elemental forms.

The chemical environment and oxidation state of the atom can be determined through the shifts of the peaks within the range expected (Table 1.9). If the electrons are shielded then it is easier, or requires less energy, to remove them from the atom, i.e., the binding energy is low. The corresponding peaks will shift to a lower energy in the expected range. If the core electrons are not shielded as much, such as the atom being in a high oxidation state, then just the opposite occurs. Similar effects occur with electronegative or electropositive elements in the chemical environment of the atom in question. By synthesizing compounds with known structures, patterns can be formed by using XPS and structures of unknown compounds can be determined.

| Compound   | Binding energy (eV) |
|--|---------------------|
| COH (C 1s)   | 286.01 – 286.8      |
| CHF (C 1s)   | 287.5 – 290.2       |
| Nitride (N 1s)   | 396.2 – 398.3       |
| Fe <sub>2</sub> O <sub>3</sub> (from O, 1s)                  | 529.5 – 530.2       |
| Fe <sub>2</sub> O <sub>3</sub> (from Fe, 2p <sub>3/2</sub> ) | 710.7 – 710.9       |
| FeO (from Fe, 2p <sub>3/2</sub> )                            | 709.1 – 709.5       |
| SiO <sub>2</sub> (from O, 1s)                                | 532.5 – 533.3       |
| SiO <sub>2</sub> (from Si, 2p)                               | 103.2 – 103.9       |

**Table 1.9:** Binding energies of electrons in various compounds.

Sample preparation is important for XPS. Although the technique was originally developed for use with thin, flat films, XPS can be used with powders. In order to use XPS with powders, a different method of sample preparation is required. One of the more common methods is to press the powder into a high purity indium foil. A different approach is to dissolve the powder in a quickly evaporating solvent, if possible, which can then be drop-casted onto a substrate. Using sticky carbon tape to adhere the powder to a disc or pressing the sample into a tablet are an option as well. Each of these sample preparations are designed to make the powder compact, as powder not attached to the substrate will contaminate the vacuum chamber. The sample also needs to be completely dry. If it is not, solvent present in the sample can destroy the necessary high vacuum and contaminate the machine, affecting the data of the current and future samples.

### 1.11.1.2 Analyzing functionalized surfaces

#### 1.11.1.2.1 Depth Profiling

When analyzing a sample (Figure 1.79 a) by XPS, questions often arise that deal with layers of the sample. For example, is the sample homogenous, with a consistent composition throughout, or layered, with certain elements or components residing in specific places in the sample? (Figure 1.79 b,c). A simple way to determine the answer to this question is to perform a depth analysis. By sputtering away the sample, data can be collected at different depths within the sample. It should be noted that sputtering is a destructive process. Within the XPS instrument, the sample is subjected to an Ar<sup>+</sup> ion beam that etches the surface. This creates a hole in the surface, allowing the X-rays to hit layers that would not have otherwise been analyzed. However, it should be realized that different surfaces and layers may be etched at different rates, meaning the same amount of etching does not occur during the same amount of time, depending on the element or compound currently being sputtered.

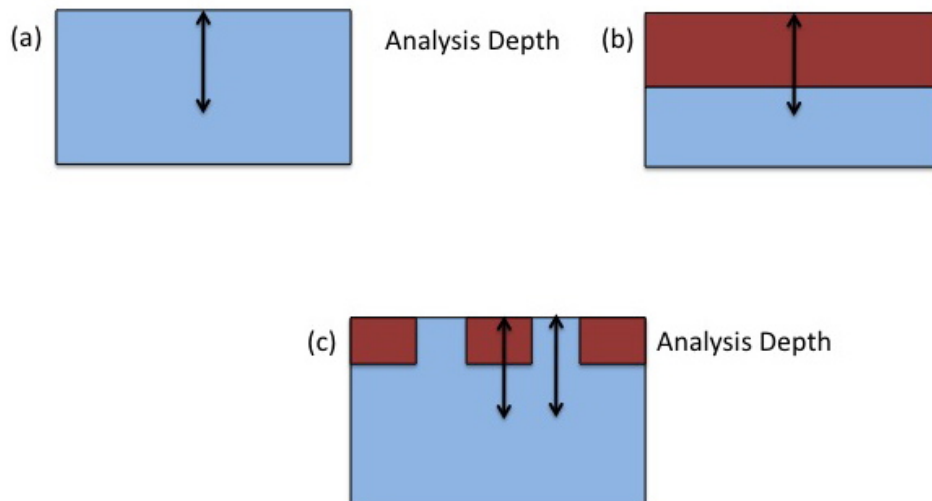


**Figure 1.79:** Schematic representation of analysis of (a) an homogeneous sample, as compared to (b) an homogeneous layers in a sample, and (c) an inhomogeneous layers in a sample.

---

It is important to note that hydrocarbons sputter very easily and can contaminate the high vacuum of the XPS instrument and thus later samples. They can also migrate to a recently sputtered (and hence unfunctionalized) surface after a short amount of time, so it is imperative to sputter and take a measurement quickly, otherwise the sputtering may appear to have had no effect.

#### 1.11.1.2.2 Functionalized Films

When running XPS, it is important that the sample is prepared correctly. If it is not, there is a high chance of ruining not only data acquisition, but the instrument as well. With organic functionalization, it is very important to ensure the surface functional group (or as is the case with many functionalized nanoparticles, the surfactant) is immobile on the surface of the substrate. If it is removed easily in the vacuum chamber, it not only will give erroneous data, but it will contaminate the machine, which may then contaminate future samples. This is particularly important when studying thiol functionalization of gold samples, as thiol groups bond strongly with the gold. If there is any loose thiol group contaminating the machine, the thiol will attach itself to any gold sample subsequently placed in the instrument, providing erroneous data. Fortunately, with the above exception, preparing samples that have been functionalized is not much different than standard preparation procedures. However, methods for analysis may have to be modified in order to obtain good, consistent data.

A common method for the analysis of surface modified material is angle resolved X-ray photoelectron spectroscopy (ARXPS). ARXPS is a non-destructive alternative to sputtering, as it relies upon using a series of small angles to analyze the top layer of the sample, giving a better picture of the surface than standard XPS. ARXPS allows for the analysis of the topmost layer of atoms to be analyzed, as opposed to standard XPS, which will analyze a few layers of atoms into the sample, as illustrated in Figure 1.80. ARXPS is often used to analyze surface contaminations, such as oxidation, and surface modification or passivation. Though the methodology and limitations are beyond the scope of this module, it is important to remember that, like normal XPS, ARXPS assumes homogeneous layers are present in samples, which can give erroneous data, should the layers be heterogeneous.

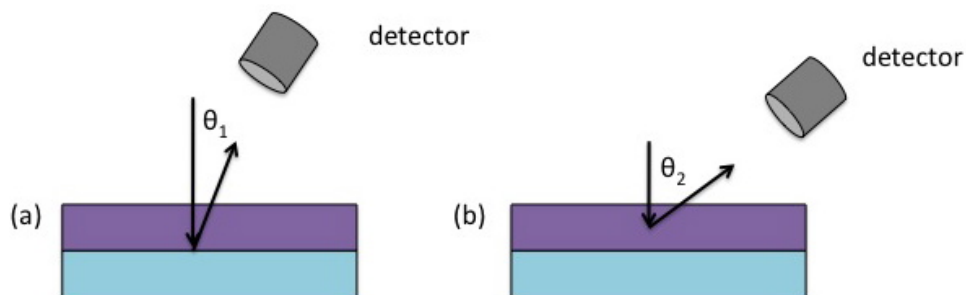


**Figure 1.80:** Schematic representation of (a) a standard XPS analysis and (b) ARXPS on a multilayer sample.

---

### 1.11.1.3 Limitations of XPS

There are many limitations to XPS that are not based on the samples or preparation, but on the machine itself. One such limitation is that XPS cannot detect hydrogen or helium. This, of course, leads to a ratio of elements in the sample that is not entirely accurate, as there is always some amount of hydrogen. It is a common fallacy to assume the percent of atoms obtained from XPS data are completely accurate due to this presence of undetected hydrogen (Table 1.8).

It is possible to indirectly measure the amount of hydrogen in a sample using XPS, but it is not very accurate and has to be done in a roundabout, often time consuming manner. If the sample contains hydrogen with a partial positive charge (i.e. OH), the sample can be washed in sodium naphthalenide ( $C_{10}H_8Na$ ). This replaces this hydrogen with sodium, which can then be measured. The sodium to oxygen ratio that is obtained infers the hydrogen to oxygen ratio, assuming that all the hydrogen atoms have reacted.

XPS can only give an average measurement, as the electrons lower down in the sample will lose more energy as they pass other atoms while the electrons on the surface retain their original kinetic energy. The electrons from lower layers can also undergo inelastic or elastic scattering, seen in Figure 1.81. This scattering may have a significant impact on data at higher angles of emission. The beam itself is also relatively wide, with the smallest width ranging from 10 – 200  $\mu m$ , lending to the observed average composition inside the beam area. Due to this, XPS cannot differentiate sections of elements if the sections are smaller than the size of the beam.

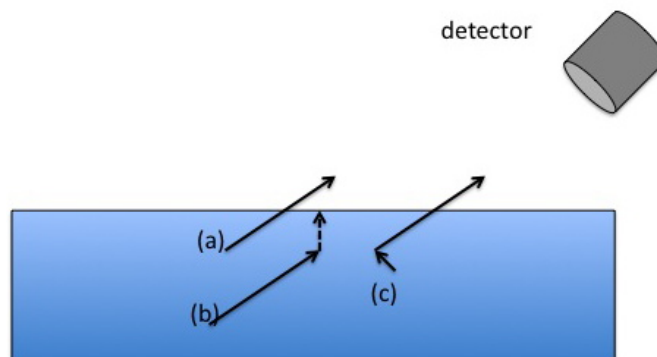


**Figure 1.81:** Schematic representation of (a) no scattering, (b) inelastic scattering, and (c) elastic scattering.

Sample reaction or degradation are important considerations. Caution should be exercised when analyzing polymers, as they are often chemically active and X-rays will provide energy to start degrading the polymer, altering the properties of the sample. One method found to help overcome this particular limitation is to use angle-resolved X-ray photoelectron spectroscopy (ARXPS). XPS can often reduce certain metal salts, such as  $\text{Cu}^{2+}$ . This reduction will give peaks that indicate a certain set of properties or chemical environments when it could be completely different. It needs to be understood that charges can build up on the surface of the sample due to a number of reasons, specifically due to the loss of electrons during the XPS experiment. The charge on the surface will interact with the electrons escaping from the sample, affecting the data obtained. If the charge collecting is positive, the electrons that have been knocked off will be attracted to the charge, slowing the electrons. The detector will pick up a lower kinetic energy of the electrons, and thus calculate a different binding energy than the one expected, giving peaks which could be labeled with an incorrect oxidation state or chemical environment. To overcome this, the spectra must be charge referenced by one of the following methods: using the naturally occurring graphite peak as a reference, sputtering with gold and using the gold peak as a reference or flooding the sample with the ion gun and waiting until the desired peak stops shifting.

#### 1.11.1.3.1 Limitations with surfactants and sputtering

While it is known that sputtering is destructive, there are a few other limitations that are not often considered. As mentioned above, the beam of X-rays is relatively large, giving an average composition in the analysis. Sputtering has the same limitation. If the surfactant or layers are not homogeneous, then when the sputtering is finished and detection begins, the analysis will show a homogeneous section, due to the size of both the beam and sputtered area, while it is actually separate sections of elements.

The chemistry of the compounds can be changed with sputtering, as it removes atoms that were bonded, changing the oxidation state of a metal or the hybridization of a non-metal. It can also introduce charges if the sample is non-conducting or supported on a non-conducting surface.

#### 1.11.1.4 Bibliography

- A. W. Apblett, A. C. Warren, and A. R. Barron, *Chem. Mater.*, 1992, 4, 167.
- A. Herrera-Gomez, J. T. Grant, P. J. Cumpson, M. Jenko, F. S. Aguirre-Tostado, C. R. Brundle, T. Conrad, G. Conti, C. S. Fadley, J. Fulghum, K. Kobayashi, L. Kövér, H. Nohira, R. L. Opila, S.

- Oswald, R. W. Paynter, R. M. Wallace, W. S. M. Werner, and J. Wolstenhorne. *Surf. Interface Anal.*, 2009, **41**, 840.
- C. C. Landry, J. A. Davis, A. W. Apblett, and A. R. Barron. *J. Mater. Chem.*, 1993, **3**, 597.
  - S. F. Mao, Z. M. Zhang, K. Tokesi, A. Csik, J. Toth, R. J. Berezky, and Z. J. Ding. *Surf. Interface Anal.*, 2008, **40**, 728.
  - J. F. Moulden, W. F. Stickle, P. E. Sobol, and K. D. Bumben. *Handbook of X-ray Photoelectron Spectroscopy*, Physical Electronics Inc. (1995).
  - J. P. Sibilía. *Materials Characterization and Chemical Analysis*, 2<sup>nd</sup> edn., Wiley–VCH (1996).

### 1.11.2 Using XPS to Analyze Metal Nanoparticles<sup>29</sup>

#### 1.11.2.1 Introduction

X-ray photoelectron spectroscopy (XPS) is a surface technique developed for use with thin films. More recently, however, it has been used to analyze the chemical and elemental composition of nanoparticles. The complication of nanoparticles is that they are neither flat nor larger than the diameter of the beam, creating issues when using the data obtained at face value. Samples of nanoparticles will often be large aggregates of particles. This creates problems with the analysis acquisition, as there can be a variety of cross-sections, as seen in Figure 1.82. This acquisition problem is also compounded by the fact that the surfactant may not be completely covering the particle, as the curvature of the particle creates defects and divots. Even if it is possible to create a monolayer of particles on a support, other issues are still present. The background support will be analyzed with the particle, due to their small size and the size of the beam and the depth at which it can penetrate.

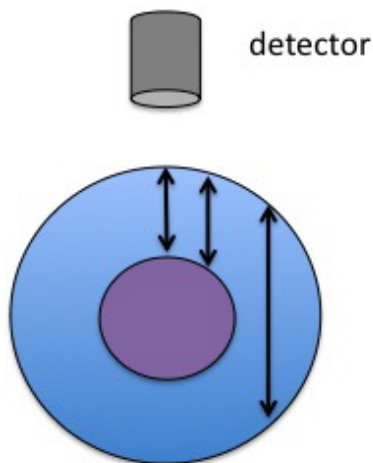


**Figure 1.82:** Different cross-sections of analysis possible on a nanoparticle.

Many other factors can introduce changes in nanoparticles and their properties. There can be probe, environmental, proximity, and sample preparation effects. The dynamics of particles can wildly vary depending on the reactivity of the particle itself. Sputtering can also be a problem. The beam used to sputter

<sup>29</sup>This content is available online at <<http://cnx.org/content/m34526/1.1/>>.

will be roughly the same size or larger than the particles. This means that what appears in the data is not a section of particle, but an average composition of several particles.

Each of these issues needs to be taken into account and preventative measures need to be used so the data is the best representation possible.

### 1.11.2.2 Sample preparation

Sample preparation of nanoparticles is very important when using XPS. Certain particles, such as iron oxides without surfactants, will interact readily with oxygen in the air. This causes the particles to gain a layer of oxygen contamination. When the particles are then analyzed, oxygen appears where it should not and the oxidation state of the metal may be changed. As shown by these particles, which call for handling, mounting and analysis without exposure to air, knowing the reactivity of the nanoparticles in the sample is very important even before starting analysis. If the reactivity of the nanoparticle is known, such as the reactivity of oxygen and iron, then preventative steps can be taken in sample preparation in order to obtain the best analysis possible.

When preparing a sample for XPS, a powder form is often used. This preparation, however, will lead to aggregation of nanoparticles. If analysis is performed on such a sample, the data obtained will be an average of composition of each nanoparticle. If composition of a single particle is what is desired, then this average composition will not be sufficient. Fortunately, there are other methods of sample preparation. Samples can be supported on a substrate, which will allow for analysis of single particles. A pictorial representation in Figure 1.83 shows the different types of samples that can occur with nanoparticles.

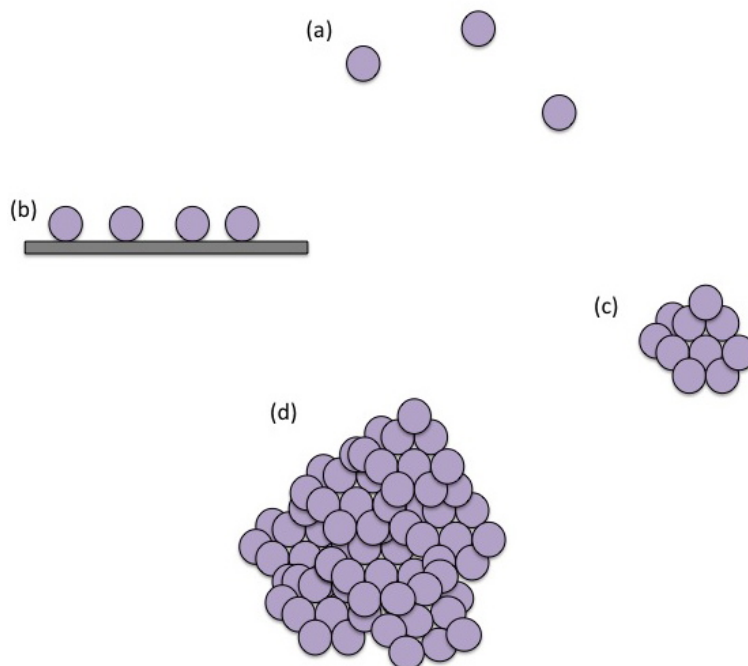


**Figure 1.83:** Representation of (a) a theoretical isolated nanoparticles, (b) nanoparticles suspended on a substrate, (c) an aggregate of nanoparticles, and (d) a powdered form of nanoparticles.

---

### 1.11.2.3 Analysis limitations

Nanoparticles are dynamic; their properties can change when exposed to new chemical environments, leading to a new set of applications. It is the dynamics of nanoparticles that makes them so useful and is one of the reasons why scientists strive to understand their properties. However, it is this dynamic ability that makes analysis difficult to do properly. Nanoparticles are easily damaged and can change properties over time or with exposure to air, light or any other environment, chemical or otherwise. Surface analysis is often difficult because of the high rate of contamination. Once the particles are inserted into XPS, even more limitations appear.

#### 1.11.2.3.1 Probe effects

There are often artifacts introduced from the simple mechanism of conducting the analysis. When XPS is used to analyze the relatively large surface of thin films, there is small change in temperature as energy is transferred. The thin films, however, are large enough that this small change in energy has to significant change to its properties. A nanoparticle is much smaller. Even a small amount of energy can drastically change the shape of particles, in turn changing the properties, giving a much different set of data than expected.

The electron beam itself can affect how the particles are supported on a substrate. Theoretically, nanoparticles would be considered separate from each other and any other chemical environments, such as solvents or substrates. This, however, is not possible, as the particles must be suspended in a solution or placed on a substrate when attempting analysis. The chemical environment around the particle will have some amount of interaction with the particle. This interaction will change characteristics of the nanoparticles, such as oxidation states or partial charges, which will then shift the peaks observed. If particles can be separated and suspended on a substrate, the supporting material will also be analyzed due to the fact that the X-ray beam is larger than the size of each individual particle. If the substrate is made of porous materials, it can adsorb gases and those will be detected along with the substrate and the particle, giving erroneous data.

#### 1.11.2.3.2 Environmental effects

Nanoparticles will often react, or at least interact, with their environments. If the particles are highly reactive, there will often be induced charges in the near environment of the particle. Gold nanoparticles have a well-documented ability to undergo plasmon interactions with each other. When XPS is performed on these particles, the charges will change the kinetic energy of the electrons, shifting the apparent binding energy. When working with nanoparticles that are well known for creating charges, it is often best to use an ion gun or a coating of gold. The purpose of the ion gun or gold coating is to try to move peaks back to their appropriate energies. If the peaks do not move, then the chance of there being no induced charge is high and thus the obtained data is fairly reliable.

#### 1.11.2.3.3 Proximity effects

The proximity of the particles to each other will cause interactions between the particles. If there is a charge accumulation near one particle, and that particle is in close proximity with other particles, the charge will become enhanced as it spreads, affecting the signal strength and the binding energies of the electrons. While the knowledge of charge enhancement could be useful to potential applications, it is not beneficial if knowledge of the various properties of individual particles is sought.

Less isolated (i.e., less crowded) particles will have different properties as compared to more isolated particles. A good example of this is the plasmon effect in gold nanoparticles. The closer gold nanoparticles are to each other, the more likely they will induce the plasmon effect. This can change the properties of the particles, such as oxidation states and partial charges. These changes will then shift peaks seen in XPS spectra. These proximity effects are often introduced in the sample preparation. This, of course, shows why it is important to prepare samples correctly to get desired results.

#### 1.11.2.4 Conclusions

Unfortunately there is no good general procedure for all nanoparticles samples. There are too many variables within each sample to create a basic procedure. A scientist wanting to use XPS to analyze nanoparticles must first understand the drawbacks and limitations of using their sample as well as how to counteract the artifacts that will be introduced in order to properly use XPS.

One must never make the assumption that nanoparticles are flat. This assumption will only lead to a misrepresentation of the particles. Once the curvature and stacking of the particles, as well as their interactions with each other are taken into account, XPS can be run.

#### 1.11.2.5 Bibliography

- D. R. Baer and M. H. Engelhard. *J. Electron Spectrosc. Rel. Phenom.*, 2009, **178-179**, 415.
- D. R. Baer, J. E. Amonette, M. H. Engelhard, D. J. Gaspar, A. S. Karakoti, S. Kuchibhatla, P. Nachimuthu, J. T. Nurmi, Y. Qiang, V. Sarathy, S. Seal, A. Sharma, P. G. Tratnyek, and C. M. Wang. *Surf. Interface Anal.*, 2008, **40**, 529.

## 1.12 Auger Electron Spectroscopy<sup>30</sup>

### 1.12.1 Basic principles

Auger electron spectroscopy (AES) is one of the most commonly employed surface analysis techniques. It uses the energy of emitted electrons to identify the elements present in a sample, similar to X-ray photoelectron spectroscopy (XPS). The main difference is that XPS uses an X-ray beam to eject an electron while AES uses an electron beam to eject an electron. In AES, the sample depth is dependent on the escape energy of the electrons. It is not a function of the excitation source as in XPS. In AES, the collection depth is limited to 1-5 nm due to the small escape depth of electrons, which permits analysis of the first 2 - 10 atomic layers. In addition, a typical analysis spot size is roughly 10 nm. A representative AES spectrum illustrating the number of emitted electrons,  $N$ , as a function of kinetic energy,  $E$ , in direct form (red) and in differentiated form (black) is shown in Figure 1.84.

---

<sup>30</sup>This content is available online at <<http://cnx.org/content/m43546/1.1/>>.

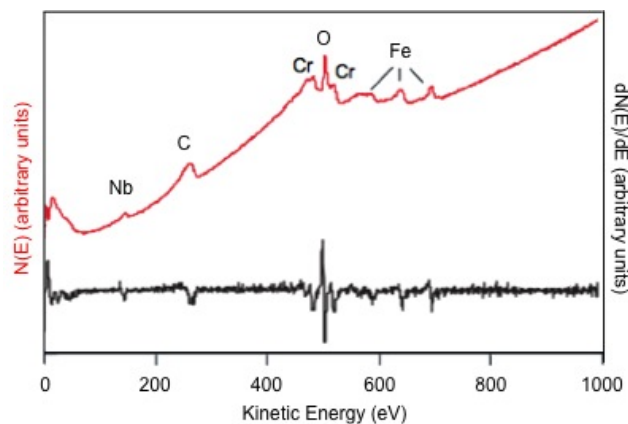


**Figure 1.84:** AES survey spectrum (red) and differentiated spectrum (black) of an oxidized Fe-Cr-Nb alloy. Adapted from H. J. Mathieu in *Surface Analysis: The Principal Techniques*, 2<sup>nd</sup> Edition, Ed. J. C. Vickerman, Wiley-VCH, Weinheim (2011).

Like XPS, AES measures the kinetic energy ( $E_k$ ) of an electron to determine its binding energy ( $E_b$ ). The binding energy is inversely proportional to the kinetic energy and can be found from (1.86), where  $h\nu$  is the energy of the incident photon and  $\Delta\Phi$  is the difference in work function between the sample and the detector material.

$$E_b = h\nu - E_k + \Delta\Phi \quad (1.86)$$

Since the  $E_b$  is dependent on the element and the electronic environment of the nucleus, AES can be used to distinguish elements and their oxidation states. For instance, the energy required to remove an electron from  $\text{Fe}^{3+}$  is more than in  $\text{Fe}^0$ . Therefore, the  $\text{Fe}^{3+}$  peak will have a lower  $E_k$  than the  $\text{Fe}^0$  peak, effectively distinguishing the oxidation states.

### 1.12.2 Auger process

An Auger electron comes from a cascade of events. First, an electron beam comes in with sufficient energy to eject a core electron creating a vacancy (see Figure 1.85A). Typical energies of the primary electrons range from 3 - 30 keV. A secondary electron (imaging electron) of higher energy drops down to fill the vacancy (see Figure 1.85B) and emits sufficient energy to eject a tertiary electron (Auger electron) from a higher shell (see Figure 1.85C).

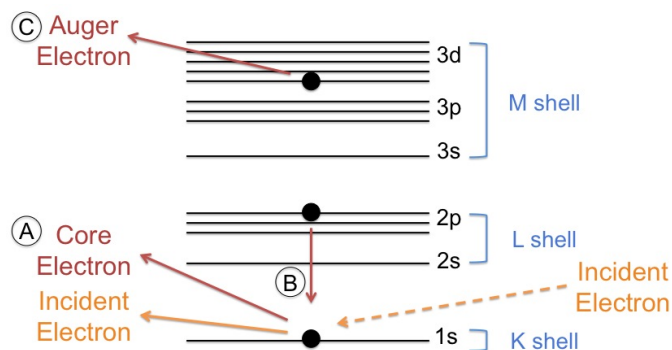


**Figure 1.85:** Schematic diagram of the Auger process.

The shells from which the electrons move from lowest to highest energy are described as the K shell, L shell, and M shell. This nomenclature is related to quantum numbers. Explicitly, the K shell represents the 1s orbital, the L shell represents the 2s and 2p orbitals, and the M shell represents the 3s, 3p, and 3d orbitals. The cascade of events typically begins with the ionization of a K shell electron, followed by the movement of an L shell electron into the K shell vacancy. Then, either an L shell electron or M shell electron is ejected. It depends on the element, which peak is prevalent but often both peaks will be present. The peak seen in the spectrum is labeled according to the shells involved in the movement of the electrons. For example, an electron ejected from a gold atom could be labeled as Au KLL or Au KLM.

The intensity of the peak depends on the amount of material present, while the peak position is element dependent. Auger transitions characteristic of each element can be found in the literature. Auger transitions of the first forty detectable elements are listed in Table 1.10.

| Atomic number | Element | AES transition | Kinetic energy of transition (eV) |
|---------------|---------|----------------|-----------------------------------|
| 3             | Li      | KLL            | 43                                |
| 4             | Be      | KLL            | 104                               |
| 5             | B       | KLL            | 179                               |
| 6             | C       | KLL            | 272                               |
| 7             | N       | KLL            | 379                               |
| 8             | O       | KLL            | 508                               |
| 9             | F       | KLL            | 647                               |

*continued on next page*

|    |    |     |      |
|----|----|-----|------|
| 11 | Na | KLL | 990  |
| 12 | Mg | KLL | 1186 |
| 13 | Al | LMM | 68   |
| 14 | Si | LMM | 92   |
| 15 | P  | LMM | 120  |
| 16 | S  | LMM | 152  |
| 17 | Cl | LMM | 181  |
| 19 | K  | KLL | 252  |
| 20 | Ca | LMM | 291  |
| 21 | Sc | LMM | 340  |
| 22 | Ti | LMM | 418  |
| 23 | V  | LMM | 473  |
| 24 | Cr | LMM | 529  |
| 25 | Mn | LMM | 589  |
| 26 | Fe | LMM | 703  |
| 27 | Co | LMM | 775  |
| 28 | Ni | LMM | 848  |
| 29 | Cu | LMM | 920  |
| 30 | Zn | LMM | 994  |
| 31 | Ga | LMM | 1070 |
| 32 | Ge | LMM | 1147 |
| 33 | As | LMM | 1228 |
| 34 | Se | LMM | 1315 |
| 35 | Br | LMM | 1376 |
| 39 | Y  | MNN | 127  |
| 40 | Zr | MNN | 147  |
| 41 | Nb | MNN | 167  |
| 42 | Mo | MNN | 186  |

**Table 1.10:** Selected AES transitions and their corresponding kinetic energy. Adapted from H. J. Mathieu in *Surface Analysis: The Principal Techniques*, Second Edition, Ed. J. C. Vickerman, Wiley-VCH, Weinheim (2011).

### 1.12.3 Instrumentation

Important elements of an Auger spectrometer include a vacuum system, an electron source, and a detector. AES must be performed at pressures less than  $10^{-3}$  pascal (Pa) to keep residual gases from adsorbing to the sample surface. This can be achieved using an ultra-high-vacuum system with pressures from  $10^{-8}$  to  $10^{-9}$  Pa. Typical electron sources include tungsten filaments with an electron beam diameter of 3 - 5  $\mu\text{m}$ , LaB<sub>6</sub> electron sources with a beam diameter of less than 40 nm, and Schottky barrier filaments with a 20 nm beam

diameter and high beam current density. Two common detectors are the cylindrical mirror analyzer and the concentric hemispherical analyzer discussed below. Notably, concentric hemispherical analyzers typically have better energy resolution.

### 1.12.3.1 Cylindrical mirror analyzer (CMA)

A CMA is composed of an electron gun, two cylinders, and an electron detector (Figure 1.86). The operation of a CMA involves an electron gun being directed at the sample. An ejected electron then enters the space between the inner and outer cylinders (IC and OC). The inner cylinder is at ground potential, while the outer cylinder's potential is proportional to the kinetic energy of the electron. Due to its negative potential, the outer cylinder deflects the electron towards the electron detector. Only electrons within the solid angle cone are detected. The resulting signal is proportional to the number of electrons detected as a function of kinetic energy.

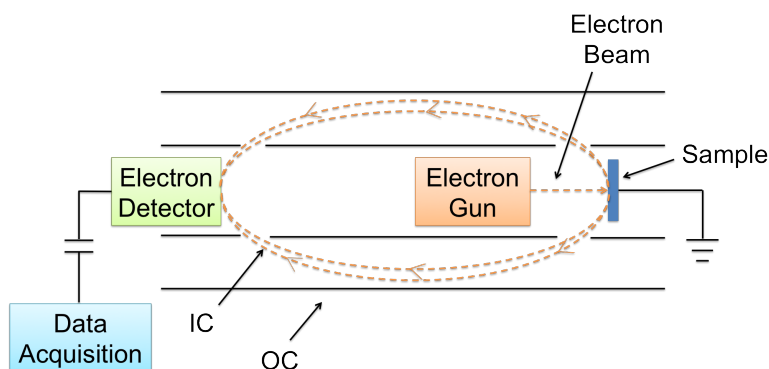


**Figure 1.86:** Schematic of a cylindrical mirror analyzer.

### 1.12.3.2 Concentric hemispherical analyzer (CHA)

A CHA contains three parts (Figure 1.87):

1. A retarding and focusing input lens assembly.
2. An inner and outer hemisphere (IH and OH).
3. An electron detector.

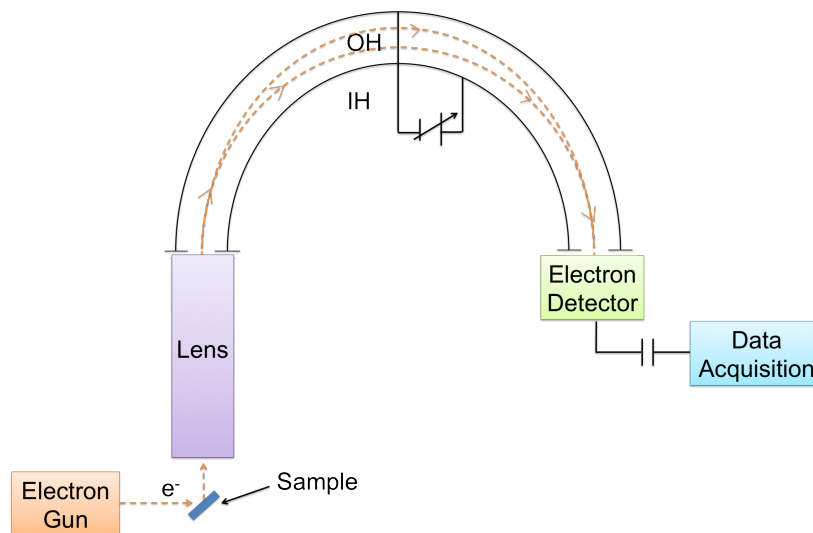


**Figure 1.87:** Schematic of a concentric hemispherical analyzer.

Electrons ejected from the surface enter the input lens, which focuses the electrons and retards their energy for better resolution. Electrons then enter the hemispheres through an entrance slit. A potential difference is applied on the hemispheres so that only electrons with a small range of energy differences reach the exit. Finally, an electron detector analyzes the electrons.

#### 1.12.4 Applications

AES has widespread use owing to its ability to analyze small spot sizes with diameters from  $5\ \mu\text{m}$  down to  $10\ \text{nm}$  depending on the electron gun. For instance, AES is commonly employed to study film growth and surface-chemical composition, as well as grain boundaries in metals and ceramics. It is also used for quality control surface analyses in integrated circuit production lines due to short acquisition times. Moreover, AES is used for areas that require high spatial resolution, which XPS cannot achieve. AES can also be used in conjunction with transmission electron microscopy (TEM) and scanning electron microscopy (SEM) to obtain a comprehensive understanding of microscale materials, both chemically and structurally. As an example of combining techniques to investigate microscale materials, Figure 1.88 shows the characterization of a single wire from a Sn-Nb multi-wire alloy. Figure 1.88a is a SEM image of the singular wire and Figure 1.88b is a schematic depicting the distribution of Nb and Sn within the wire. Point analysis was performed along the length of the wire to determine the percent concentrations of Nb and Sn.

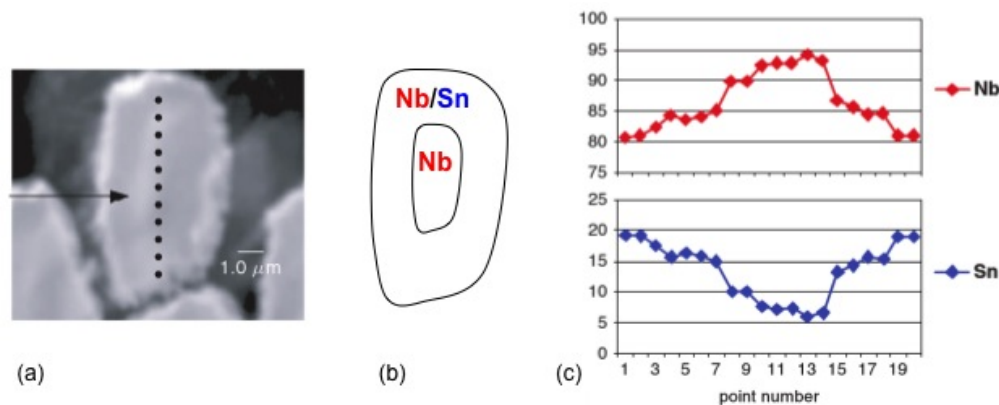


**Figure 1.88:** Analysis of a Sn-Nb wire. (a) SEM image of the wire, (b) schematic of the elemental distribution, and (c) graphical representation of point analysis giving the percent concentration of Nb and Sn. Adapted from H. J. Mathieu in *Surface Analysis: The Principal Techniques*, Second Edition, Ed. J. C. Vickerman, Wiley-VCH, Weinheim (2011).

AES is widely used for depth profiling. Depth profiling allows the elemental distributions of layered samples  $0.2 - 1 \mu\text{m}$  thick to be characterized beyond the escape depth limit of an electron. Varying the incident and collection angles, and the primary beam energy controls the analysis depth. In general, the depth resolution decreases with the square root of the sample thickness. Notably, in AES, it is possible to simultaneously sputter and collect Auger data for depth profiling. The sputtering time indicates the depth and the intensity indicates elemental concentrations. Since, the sputtering process does not affect the ejection of the Auger electron, helium or argon ions can be used to sputter the surface and create the trench, while collecting Auger data at the same time. The depth profile does not have the problem of diffusion of hydrocarbons into the trenches. Thus, AES is better for depth profiles of reactive metals (e.g., gold or any metal or semiconductor). Yet, care should be taken because sputtering can mix up different elements, changing the sample composition.

### 1.12.5 Limitations

While AES is a very valuable surface analysis technique, there are limitations. Because AES is a three-electron process, elements with less than three electrons cannot be analyzed. Therefore, hydrogen and helium cannot be detected. Nonetheless, detection is better for lighter elements with fewer transitions. The numerous transition peaks in heavier elements can cause peak overlap, as can the increased peak width of higher energy transitions. Detection limits of AES include  $0.1 - 1\%$  of a monolayer,  $10^{-16} - 10^{-15}$  g of material, and  $10^{12} - 10^{13}$  atoms/cm<sup>2</sup>.

Another limitation is sample destruction. Although focusing of the electron beam can improve resolution; the high-energy electrons can destroy the sample. To limit destruction, beam current densities of greater than  $1 \text{ mA/cm}^2$  should be used. Furthermore, charging of the electron beam on insulating samples can deteriorate the sample and result in high-energy peak shifts or the appearance of large peaks.

### 1.12.6 Bibliography

- H. Bubert, J. Rivière, and W. Werner, *Surface and Thin Film Analysis: A Compendium of Principles, Instrumentation, and Applications*, Second Edition, Ed. G. Friedbacher and H. Bubert, Wiley-VCH,

Weinheim (2011).

- H. Lüth in *Solid Surfaces, Interfaces and Thin Films*, Fifth Edition, Springer, New York (2010).
- H. J. Mathieu in *Surface Analysis: The Principal Techniques*, Second Edition, Ed. J. C. Vickerman, Wiley-VCH, Weinheim (2011).
- S. N. Raman, D. F. Paul, J. S. Hammond, and K. D. Bomben, *Microscopy Today*, 2011, **19**, 12.
- N. Turner in *Analytical Instrumentation Handbook*, Second Edition, Ed. G. Ewing, Marcel Dekker, Inc, New York (1997).
- J. F. Watts in *Handbook of Adhesion Technology*, Ed. Lucas F.M. da Silva, A. Öchsner, and R. Adams, Springer, New York (2011).
- V. Young and G. Hoflund in *Handbook of Surface and Interface Analysis Methods for Problem-Solving*, Second Edition, Ed. J. Rivière and S. Myhra, CRC Press, Boca Raton (2009).

## 1.13 Rutherford Backscattering of Thin Films<sup>31</sup>

### 1.13.1 Introduction

One of the main research interests of the semiconductor industry is to improve the performance of semi-conducting devices and to construct new materials with reduced size or thickness that have potential application in transistors and microelectronic devices. However, the most significant challenge regarding thin film semiconductor materials is measurement. Properties such as the thickness, composition at the surface, and contamination, all are critical parameters of the thin films. To address these issues, we need an analytical technique which can measure accurately through the depth of the of the semiconductor surface without destruction of the material. Rutherford backscattering spectroscopy is a unique analysis method for this purpose. It can give us information regarding in-depth profiling in a non-destructive manner. However X-ray photo electron spectroscopy (XPS), energy dispersive X-ray analysis (EDX) and Auger electron spectroscopy are also able to study the depth-profile of semiconductor films. Table 1.11 demonstrates the comparison between those techniques with RBS.

| Method | Destructive | Incident particle | Outgoing Particle | Detection limit | Depth resolution |
|--------|-------------|-------------------|-------------------|-----------------|------------------|
| RBS    | No          | Ion               | Ion               | ~1              | 10 nm            |
| XPS    | Yes         | X-ray photon      | Electron          | ~0.1-1          | ~1 $\mu\text{m}$ |
| EDX    | Yes         | Electron          | X-ray photon      | ~0.1            | 1.5 nm           |
| Auger  | Yes         | Electron          | Electron          | ~0.1-1          | 1.5 nm           |

Table 1.11: Comparison between different thin film analysis techniques.

### 1.13.2 Basic concept of Rutherford backscattering spectroscopy

At a basic level, RBS demonstrates the electrostatic repulsion between high energy incident ions and target nuclei. The specimen under study is bombarded with monoenergetic beam of  $^4\text{He}^+$  particles and the backscattered particles are detected by the detector-analysis system which measures the energies of the particles. During the collision, energy is transferred from the incident particle to the target specimen atoms; the change in energy of the scattered particle depends on the masses of incoming and target atoms. For an incident particle of mass  $M_1$ , the energy is  $E_0$  while the mass of the target atom is  $M_2$ . After the collision, the residual energy  $E$  of the particle scattered at angle  $\theta$  can be expressed as:

<sup>31</sup>This content is available online at <<http://cnx.org/content/m22411/1.3/>>.

$$E = k^2 E_0$$

$$k = \frac{\left( M_1 \cos \varnothing + \sqrt{M_2^2 - M_1^2 \sin^2 \varnothing} \right)}{M_1 + M_2}$$

where  $k$  is the kinematic scattering factor, which is actually the energy ratio of the particle before and after the collision. Since  $k$  depends on the masses of the incident particle and target atom and the scattering angle, the energy of the scattered particle is also determined by these three parameters. A simplified layout of backscattering experiment is shown in Figure 1 (Figure 1.89).

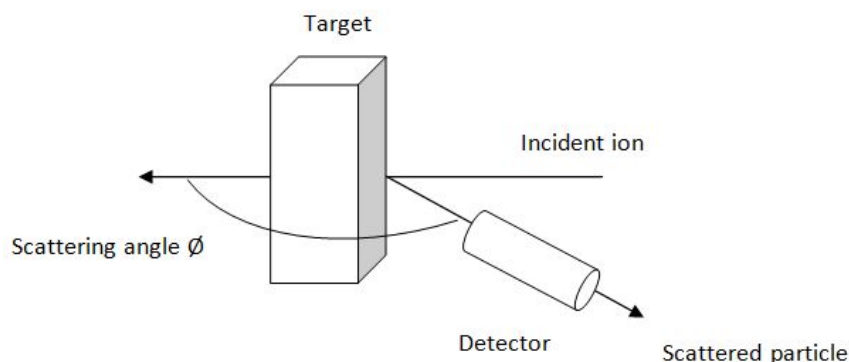


**Figure 1.89:** Schematic representation of the experimental setup for Rutherford backscattering analysis.

The probability of a scattering event can be described by the differential scattering cross section of a target atom for scattering an incoming particle through the angle  $\varnothing$  into differential solid angle as follows,

$$\frac{d\sigma_R}{d\varphi} = \left( \frac{zZe^2}{2E_0 \sin^2 \varnothing} \right) \frac{\left[ \cos \varnothing + \sqrt{1 - \left( \frac{M_1}{M_2} \sin \varnothing \right)^2} \right]^2}{\sqrt{1 - \left( \frac{M_1}{M_2} \sin \varnothing \right)^2}}$$

where  $d\sigma_R$  is the effective differential cross section for the scattering of a particle. The above equation may look complicated but it conveys the message that the probability of scattering event can be expressed as a function of scattering cross section which is proportional to the  $zZ$  when a particle with charge  $ze$  approaches the target atom with charge  $Ze$ .

Helium ions not scattered at the surface lose energy as they traverse the solid. They lose energy due to interaction with electrons in the target. After collision the He particles lose further energy on their way out to the detector. We need to know two quantities to measure the energy loss, the distance  $\Delta t$  that the particles penetrate into the target and the energy loss  $\Delta E$  in this distance Figure 1.90. The rate of energy loss or stopping power is a critical component in backscattering experiments as it determines the depth profile in a given experiment.

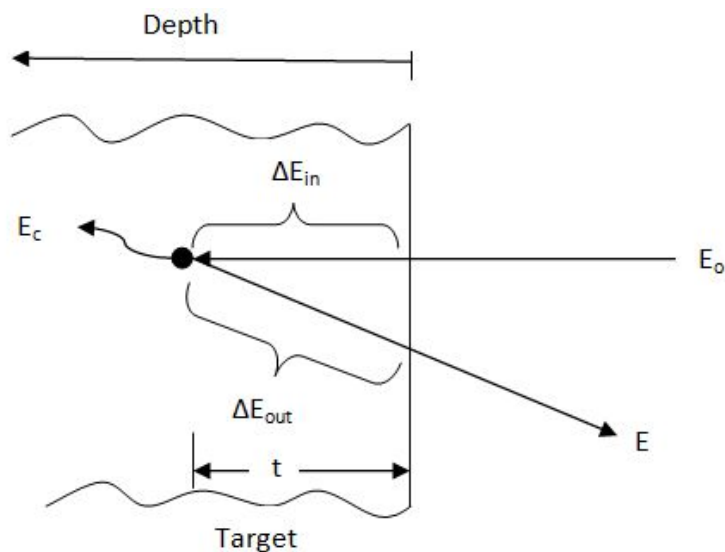


**Figure 1.90:** Components of energy loss for a ion beam that scatters from depth  $t$ . First, incident beam loses energy through interaction with electrons  $\Delta E_{in}$ . Then energy lost occurs due to scattering  $E_c$ . Finally outgoing beam loses energy for interaction with electrons  $\Delta E_{out}$ . Adapted from L. C. Feldman and J. W. Mayer, *Fundamentals of Surface and Thin Film Analysis*, North Holland-Elsevier, New York (1986).

In thin film analysis, it is convenient to assume that total energy loss  $\Delta E$  into depth  $t$  is only proportional to  $t$  for a given target. This assumption allows a simple derivation of energy loss in backscattering as more complete analysis requires many numerical techniques. In constant  $dE/dx$  approximation, total energy loss becomes linearly related to depth  $t$ , Figure 1.91.

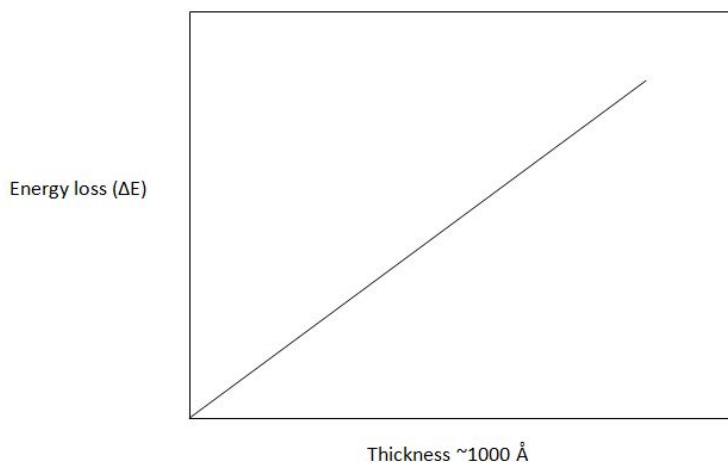


**Figure 1.91:** Variation of energy loss with the depth of the target in constant  $dE/dx$  approximation.

---

### 1.13.3 Experimental set-up

The apparatus for Rutherford backscattering analysis of thin solid surface typically consist of three components:

1. A source of helium ions.
2. An accelerator to energize the helium ions.
3. A detector to measure the energy of scattered ions.

There are two types of accelerator/ion source available. In single stage accelerator, the  $\text{He}^+$  source is placed within an insulating gas-filled tank (Figure 1.92). It is difficult to install new ion source when it is exhausted in this type of accelerator. Moreover, it is also difficult to achieve particles with energy much more than 1 MeV since it is difficult to apply high voltages in this type of system.

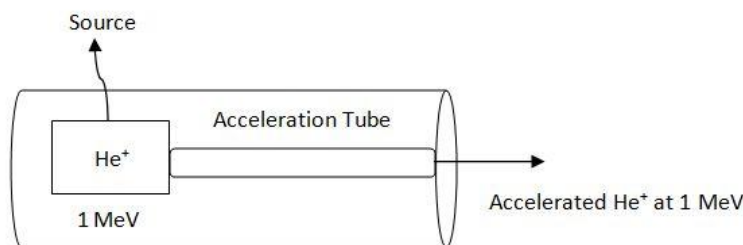


**Figure 1.92:** Schematic representation of a single stage accelerator.

---

Another variation is “tandem accelerator.” Here the ion source is at ground and produces negative ion. The positive terminal is located at the center of the acceleration tube (Figure 1.93). Initially the negative ion is accelerated from ground to terminal. At terminal two-electron stripping process converts the  $\text{He}^-$  to  $\text{He}^{++}$ . The positive ions are further accelerated toward ground due to columbic repulsion from positive terminal. This arrangement can achieve highly accelerated  $\text{He}^{++}$  ions ( $\sim 2.25$  MeV) with moderate voltage of 750 kV.

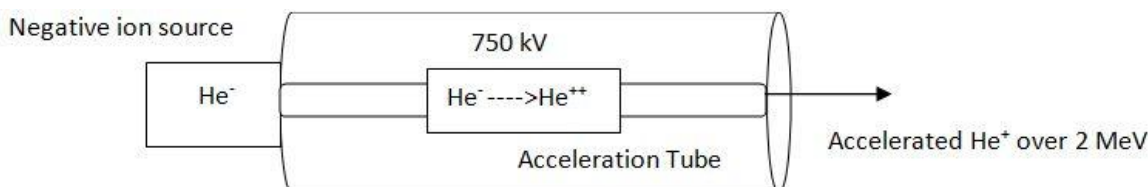


**Figure 1.93:** Schematic representation of a tandem accelerator.

---

Particles that are backscattered by surface atoms of the bombarded specimen are detected by a surface barrier detector. The surface barrier detector is a thin layer of p-type silicon on the n-type substrate resulting p-n junction. When the scattered ions exchange energy with the electrons on the surface of the detector upon reaching the detector, electrons get promoted from the valence band to the conduction band. Thus, each exchange of energy creates electron-hole pairs. The energy of scattered ions is detected by simply counting the number of electron-hole pairs. The energy resolution of the surface barrier detector in a standard RBS experiment is 12 - 20 keV. The surface barrier detector is generally set between  $90^\circ$  and  $170^\circ$  to the incident beam. Films are usually set normal to the incident beam. A simple layout is shown in Figure 1.94.

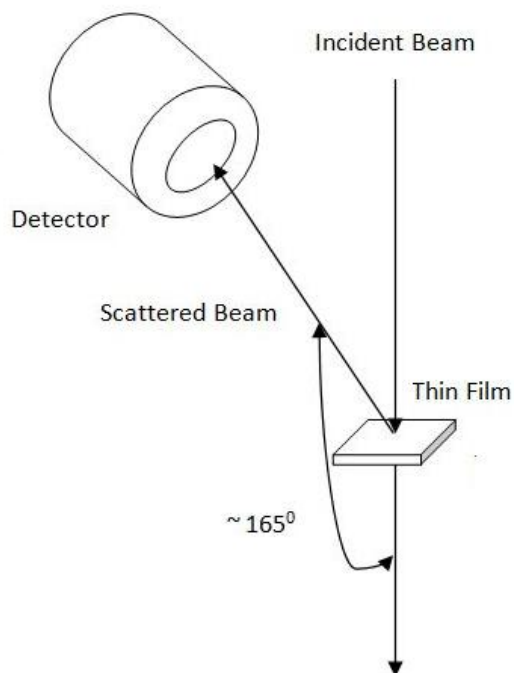


**Figure 1.94:** Schematic representation general setup where the surface barrier detector is placed at angle of  $165^\circ$  to the extrapolated incident beam.

#### 1.13.4 Depth profile analysis

As stated earlier, it is a good approximation in thin film analysis that the total energy loss  $\Delta E$  is proportional to depth  $t$ . With this approximation, we can derive the relation between energy width  $\Delta E$  of the signal from a film of thickness  $\Delta t$  as follows,

$$\Delta E = \Delta t (k \frac{dE}{dx}_{in} + \frac{1}{\cos \emptyset} \frac{dE}{dx}_{out})$$

where  $\emptyset$  = lab scattering angle.

It is worth noting that  $k$  is the kinematic factor defined in equation above and the subscripts “in” and “out” indicate the energies at which the rate of loss of energy or  $dE/dx$  is evaluated. As an example, we consider the backscattering spectrum, at scattering angle  $170^\circ$ , for 2 MeV  $\text{He}^{++}$  incidents on silicon layer deposited onto 2 mm thick niobium substrate Figure 1.95.

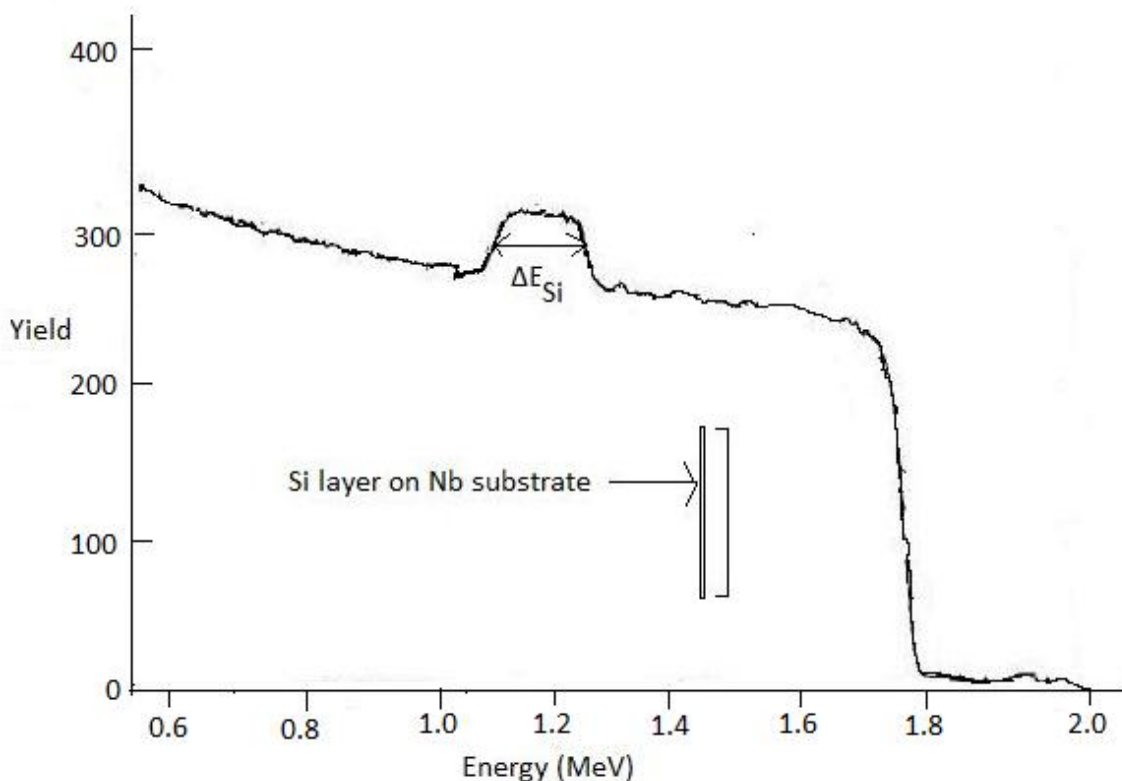


**Figure 1.95:** The backscattering spectrum for 2.0 MeV He ions incident on a silicon thin film deposited onto a niobium substrate. Adapted from P. D. Stupik, M. M. Donovan, A. R. Barron, T. R. Jervis and M. Nastasi, *Thin Solid Films*, 1992, **207**, 138.

The energy loss rate of incoming  $\text{He}^{++}$  or  $dE/dx$  along inward path in elemental Si is  $\approx 24.6 \text{ eV}/\text{\AA}$  at 2 MeV and is  $\approx 26 \text{ eV}/\text{\AA}$  for the outgoing particle at 1.12 MeV (Since  $K$  of Si is 0.56 when the scattering angle is  $170^\circ$ , energy of the outgoing particle would be equal to  $2 \times 0.56$  or 1.12 MeV). Again the value of  $\Delta E_{\text{Si}}$  is  $\approx 133.3 \text{ keV}$ . Putting the values into above equation we get

$$\begin{aligned} \Delta t &\approx 133.3 \text{ keV} / (0.56 * 24.6 \text{ eV}/\text{\AA} + 1/\cos 170^\circ * 26 \text{ eV}/\text{\AA}) \\ &= 133.3 \text{ keV} / (13.77 \text{ eV}/\text{\AA} + 29.985 \text{ eV}/\text{\AA}) \\ &= 133.3 \text{ keV} / 40.17 \text{ eV}/\text{\AA} \\ &= 3318 \text{ \AA} \end{aligned}$$

Hence a Si layer of ca. 3300  $\text{\AA}$  thickness has been deposited on the niobium substrate. However we need to remember that the value of  $dE/dx$  is approximated in this calculation.

### 1.13.5 Quantitative Analysis

In addition to depth profile analysis, we can study the composition of an element quantitatively by backscattering spectroscopy. The basic equation for quantitative analysis is

$$Y = \sigma \cdot \Omega \cdot Q \cdot N \Delta t$$

Where  $Y$  is the yield of scattered ions from a thin layer of thickness  $\Delta t$ ,  $Q$  is the number of incident ions and  $\Omega$  is the detector solid angle, and  $N\Delta t$  is the number of specimen atoms ( $\text{atom}/\text{cm}^2$ ). shows the RBS spectrum for a sample of silicon deposited on a niobium substrate and subjected to laser mixing. The Nb has reacted with the silicon to form a  $\text{NbSi}_2$  interphase layer. The Nb signal has broadened after the reaction as show in .

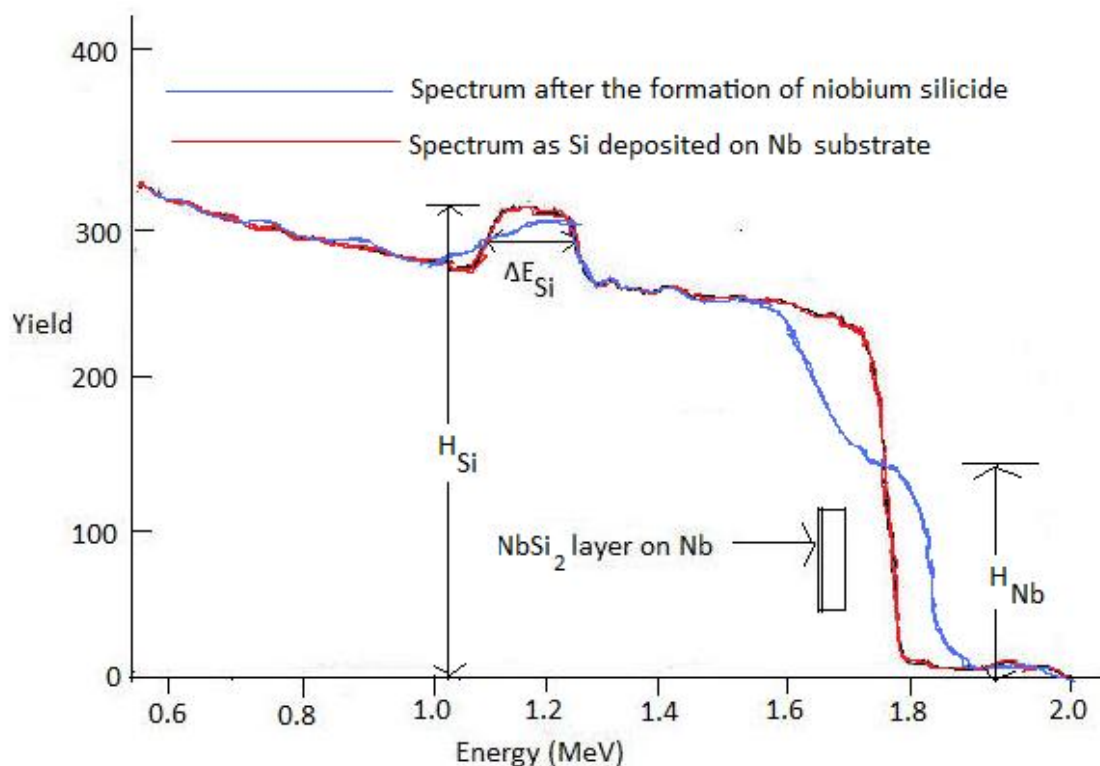


**Figure 1.96:** Backscattering spectra of Si diffused into Nb and Si as deposited on Nb substrate. Adapted from P. D. Stupik, M. M. Donovan, A. R. Barron, T. R. Jervis and M. Nastasi, *Thin Solid Films*, 1992, 207, 138.

We can use ratio of the heights  $H_{\text{Si}}/H_{\text{Nb}}$  of the backscattering spectrum after formation of  $\text{NbSi}_2$  to determine the composition of the silicide layer. The stoichiometric ratio of Nb and Si can be approximated as,

$$N_{\text{Si}}/N_{\text{Nb}} \approx [H_{\text{Si}} * \sigma_{\text{Si}}]/[H_{\text{Nb}} * \sigma_{\text{Nb}}]$$

Hence the concentration of Si and Nb can be determined if we can know the appropriate cross sections  $\sigma_{\text{Si}}$  and  $\sigma_{\text{Nb}}$ . However the yield in the backscattering spectra is better represented as the product of signal height and the energy width  $\Delta E$ . Thus stoichiometric ratio can be better approximated as

$$N_{\text{Si}}/N_{\text{Nb}} \approx [H_{\text{Si}} * \Delta E_{\text{Si}} * \sigma_{\text{Si}}]/[H_{\text{Nb}} * \Delta E_{\text{Nb}} * \sigma_{\text{Nb}}]$$

### 1.13.6 Limitations

It is of interest to understand the limitations of the backscattering technique in terms of the comparison with other thin film analysis technique such as AES, XPS and SIMS (Table 1.11). AES has better mass resolution, lateral resolution and depth resolution than RBS. But AES suffers from sputtering artifacts. Compared to RBS, SIMS has better sensitivity. RBS does not provide any chemical bonding information which we can get from XPS. Again, sputtering artifact problems are also associated in XPS. The strength of RBS lies in quantitative analysis. However, conventional RBS systems cannot analyze ultrathin films since the depth resolution is only about 10 nm using surface barrier detector.

### 1.13.7 Summary

Rutherford Backscattering analysis is a straightforward technique to determine the thickness and composition of thin films ( $< 4000 \text{ \AA}$ ). Areas that have been lately explored are the use of backscattering technique in composition determination of new superconductor oxides; analysis of lattice mismatched epitaxial layers, and as a probe of thin film morphology and surface clustering.

### 1.13.8 Bibliography

- L. C. Feldman and J. W. Mayer, *Fundamentals of Surface and Thin Film Analysis*, North Holland-Elsevier, New York (1986).
- *Ion Spectroscopies for Surface Analysis*, Ed. A. W. Czanderna and D. M. Hercules, Plenum Press (New York), 1991.
- P. D. Stupik, M. M. Donovan, A. R. Barron, T. R. Jervis, and M. Nastasi, *Thin Solid Films*, 1992, **207**, 138

## 1.14 An Accuracy Assessment of the Refinement of Crystallographic Positional Metal Disorder in Molecular Solid Solutions<sup>32</sup>

### 1.14.1 Introduction

Crystallographic positional disorder is evident when a position in the lattice is occupied by two or more atoms; the average of which constitutes the bulk composition of the crystal. If a particular atom occupies a certain position in one unit cell and another atom occupies the same position in other unit cells, the resulting electron density will be a weight average of the situation in all the unit cells throughout the crystal. Since the diffraction experiment involves the average of a very large number of unit cells (*ca.*  $10^{18}$  in a crystal used for single crystal X-ray diffraction analysis), minor static displacements of atoms closely simulate the effects of vibrations on the scattering power of the "average" atom. Unfortunately, the determination of the "average" atom in a crystal may be complicated if positional disorder is encountered.

Crystal disorder involving groups such as CO, CN and Cl have been documented to create problems in assigning the correct structure through refinement procedures. While attempts have been made to correlate crystallographic lattice parameters with bulk chemical composition of the solution from which single crystal was grown, there has been little effort to correlate crystallographic site occupancy with chemical composition of the crystal from which single crystal diffraction data was obtained. These are two very different issues that must be considered when solving a crystal structure with site occupancy disorder.

1. What is the relationship of a single crystal to the bulk material?
2. Is the refinement of a site-occupancy-factor actually gives a realistic value for % occupancy when compared to the "actual" % composition for that particular single crystal?

<sup>32</sup>This content is available online at <http://cnx.org/content/m26148/1.2/>.

The following represents a description of a series of methods for the refinement of a site occupancy disorder between two atoms (e.g., two metal atoms within a mixture of isostructural compounds).

### 1.14.2 Methods for X-ray diffraction determination of positional disorder in molecular solid solutions

An atom in a structure is defined by several parameters: the type of atom, the positional coordinates (x, y, z), the occupancy factor (how many “atoms” are at that position) and atomic displacement parameters (often called temperature or thermal parameters). The latter can be thought of as being a “picture” of the volume occupied by the atom over all the unit cells, and can be isotropic (1 parameter defining a spherical volume) or anisotropic (6 parameters defining an ellipsoidal volume). For a “normal” atom, the occupancy factor is fixed as being equal to one, and the positions and displacement parameters are “refined” using least-squares methods to values in which the best agreement with the observed data is obtained. In crystals with site-disorder, one position is occupied by different atoms in different unit cells. This refinement requires a more complicated approach. Two broad methods may be used: either a new atom type that is the appropriate combination of the different atoms is defined, or the same positional parameters are used for different atoms in the model, each of which has occupancy values less than one, and for which the sum is constrained to total one. In both approaches, the relative occupancies of the two atoms are required. For the first approach, these occupancies have to be defined. For the second, the value can be refined. However, there is a relationship between the thermal parameter and the occupancy value so care must be taken when doing this. These issues can be addressed in several ways.

#### 1.14.2.1 Method 1

The simplest assumption is that the crystal from which the X-ray structure is determined represents the bulk sample was crystallized. With this value, either a new atom type can be generated that is the appropriate combination of the measured atom type 1 (M) and atom type 2 (M') percent composition or two different atoms can be input with the occupancy factor set to reflect the percent composition of the bulk material. In either case the thermal parameters can be allowed to refine as usual.

#### 1.14.2.2 Method 2

The occupancy values for two atoms (M and M') are refined (such that their sum was equal to 1), while the two atoms are constrained to have the same displacement parameters.

#### 1.14.2.3 Method 3

The occupancy values (such that their sum was equal to 1) and the displacement parameters are refined independently for the two atoms.

#### 1.14.2.4 Method 4

Once the best values for occupancy is obtained using either Methods 2 or 3, these values were fixed and the displacement parameters are allowed to refine freely.

### 1.14.3 A model system

Metal  $\beta$ -diketonate complexes (Figure 1.97) for metals in the same oxidation state are isostructural and often isomorphous. Thus, crystals obtained from co-crystallization of two or more metal  $\beta$ -diketonate complexes [e.g.,  $\text{Al}(\text{acac})_3$  and  $\text{Cr}(\text{acac})_3$ ] may be thought of as a hybrid of the precursors; that is, the metal position in the crystal lattice may be defined as having the average metal composition.

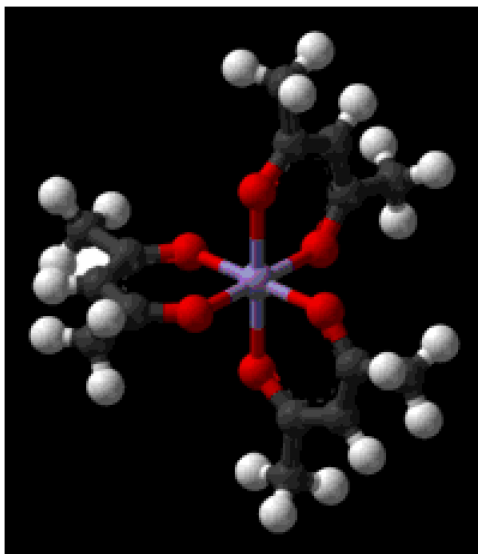


**Figure 1.97:** Molecular structure of  $M(\text{acac})_3$ , a typical metal  $\beta$ -diketonate complex.

A series of solid solutions of  $\text{Al}(\text{acac})_3$  and  $\text{Cr}(\text{acac})_3$  can be prepared for study by X-ray diffraction, by the crystallization from acetone solutions of specific mixtures of  $\text{Al}(\text{acac})_3$  and  $\text{Cr}(\text{acac})_3$  (Table 1.12, Column 1). The pure derivatives and the solid solution,  $\text{Al}_{1-x}\text{Cr}_x(\text{acac})_3$ , crystallize in the monoclinic space group  $P2_1/c$  with  $Z = 4$ .

| Solution composition (% Cr) | WDS composition of single crystal (% Cr) | Composition as refined from X-ray diffraction (% Cr) |
|-----------------------------|--|--|
| 13                          | $1.9 \pm 0.2$                            | 0 <sup>a</sup>                                       |
| 2                           | $2.1 \pm 0.3$                            | 0 <sup>a</sup>                                       |
| 20                          | $17.8 \pm 1.6$                           | $17.3 \pm 1.8$                                       |
| 26                          | $26.7 \pm 1.7$                           | $28.3 \pm 1.9$                                       |
| 18                          | $48.5 \pm 4.9$                           | $46.7 \pm 2.1$                                       |
| 60                          | $75.1 \pm 4.1$                           | $72.9 \pm 2.4$                                       |
| 80                          | $91.3 \pm 1.2$                           | $82.3 \pm 3.1$                                       |

**Table 1.12:** Variance in chromium concentrations (%) for samples of  $\text{Al}_{1-x}\text{Cr}_x(\text{acac})_3$  crystallized from solutions of  $\text{Al}(\text{acac})_3$  and  $\text{Cr}(\text{acac})_3$ . <sup>a</sup>Concentration too low to successfully refine the Cr occupancy.

Substitution of Cr for Al in the  $M(\text{acac})_3$  structure could possibly occur in a random manner, i.e., a metal site has an equal probability of containing an aluminum or a chromium atom. Alternatively, if the chromium had preference for specific sites a super lattice structure of lower symmetry would be present. Such an ordering is not observed since all the samples show no additional reflections other than those that may be indexed to the monoclinic cell. Therefore, it may be concluded that the  $\text{Al}(\text{acac})_3$  and  $\text{Cr}(\text{acac})_3$  do indeed form solid solutions:  $\text{Al}_{1-x}\text{Cr}_x(\text{acac})_3$ .

Electron microprobe analysis, using wavelength-dispersive spectrometry (WDS), on the individual crystal from which X-ray crystallographic data was collected provides the “actual” composition of each crystal. Analysis was performed on at least 6 sites on each crystal using a 10  $\mu\text{m}$  sized analysis spot providing a measure of the homogeneity within the individual crystal for which X-ray crystallographic data was collected. An example of a SEM image of one of the crystals and the point analyses is given in Figure 1.98. The data in Table 1.12 and Figure 1.98 demonstrate that while a batch of crystals may contain individual crystals with different compositions, each individual crystal is actually reasonably homogenous. There is, for most samples, a significant variance between the molar Al:Cr ratio in the bulk material and an individual crystal chosen for X-ray diffraction. The variation in Al:Cr ratio within each individual crystal ( $\pm 10\%$ ) is much less than that between crystals.

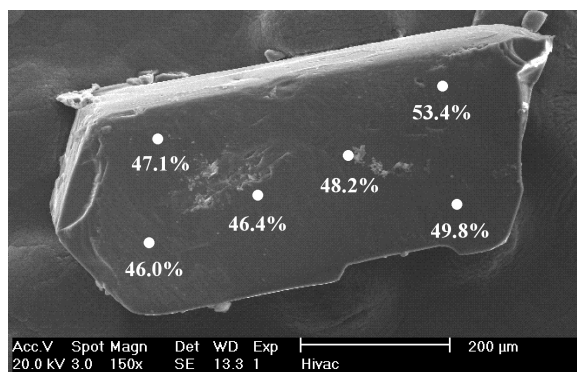


**Figure 1.98:** SEM image of a representative crystal used for WDS and X-ray diffraction analysis showing the location and results for the WDS analysis. The 10  $\mu\text{m}$  sized analysis spots are represented by the white dots. Adapted from B. D. Fahlman, Ph.D. Thesis, Rice University, 2000.

## 1.14.4 Comparison of the methods

### 1.14.4.1 Method 1

Since Method 1 does not refine the %Cr and relies on an input for the Al and Cr percent composition of the "bulk" material, i.e., the %Cr in the total mass of the material (Table 1.12, Column 1), as opposed to the analysis of the single crystal on which X-ray diffraction was performed, (Table 1.12, Column 2), the closer these values were to the "actual" value determined by WDS for the crystal on which X-ray diffraction was performed (Table 1.12, Column 1 versus 2) then the closer the overall refinement of the structure to those of Methods 2 - 4.

While this assumption is obviously invalid for many of the samples, it is one often used when bulk data (for example, from NMR) is available. However, as there is no reason to assume that one crystal is completely representative of the bulk sample, it is unwise to rely only on such data.

### 1.14.4.2 Method 2

This method always produced final, refined, occupancy values that were close to those obtained from WDS (Table 1.12). This approach assumes that the motion of the central metal atoms is identical. While this is obviously not strictly true as they are of different size, the results obtained herein imply that this is a reasonable approximation where simple connectivity data is required. For samples where the amount of one

of the elements (i.e., Cr) is very low so low a good refinement can not often be obtained. In these cases, when refining the occupancy values, that for Al would exceed 1 while that of Cr would be less than 1!

#### 1.14.4.3 Method 3

In some cases, despite the interrelationship between the occupancy and the displacement parameters, convergence was obtained successfully. In these cases the refined occupancies were both slightly closer to those observed from WDS than the occupancy values obtained using Method 2. However, for some samples with higher Cr content the refinement was unstable and would not converge. Whether this observation was due to the increased percentage of Cr or simply lower data quality is not certain.

While this method does allow refinement of any differences in atomic motion between the two metals, it requires extremely high quality data for this difference to be determined reliably.

#### 1.14.4.4 Method 4

This approach adds little to the final results.

#### 1.14.5 Correlation between analyzed composition and refined composition

Figure 1.99 shows the relationship between the chromium concentration (%Cr) determined from WDS and the refinement of X-ray diffraction data using Methods 2 or 3 (labeled in Figure 1.99). Clearly there exists a good correlation, with only a slight divergence at high Cr concentration. This is undoubtedly a consequence of trying to refine a low fraction of a light atom (Al) in the presence of a large fraction of a heavier atom (Cr). X-ray diffraction is, therefore, an accurate method of determining the M:M' ratios in crystalline solid solution.

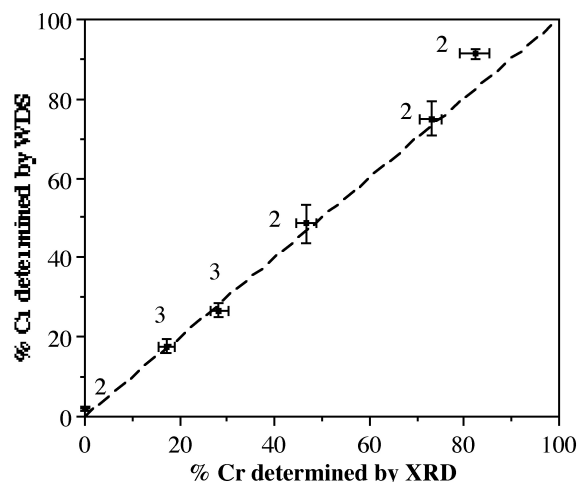


**Figure 1.99:** Comparison of the chromium concentration determined from WDS (with error) and refinement of X-ray diffraction data (with error) using Methods 2 or 3. Adapted from S. G. Bott, B. D. Fahlman, M. L. Pierson, and A. R. Barron, *J. Chem. Soc., Dalton Trans.*, 2001, 2148.

---

### 1.14.6 Bibliography

- S. G. Bott, B. D. Fahlman, M. L. Pierson, and A. R. Barron, *J. Chem. Soc., Dalton Trans.*, 2001, 2148.
- K. R. Dunbar and S. C. Haefner, *Inorg. Chem.*, 1992, **31**, 3676.
- J. Glusker, M. Lewis, and M., Rossi, *Crystal Structure Analysis for Chemists and Biologists* VCH: New York (1994).
- K. Yoon and G. Parkin, *Inorg. Chem.*, 1992, **114**, 31.

## 1.15 Principles of Gamma-ray Spectroscopy and Applications in Nuclear Forensics<sup>33</sup>

### 1.15.1 Introduction

Gamma-ray ( $\gamma$ -ray) spectroscopy is a quick and nondestructive analytical technique that can be used to identify various radioactive isotopes in a sample. In gamma-ray spectroscopy, the energy of incident gamma-rays is measured by a detector. By comparing the measured energy to the known energy of gamma-rays produced by radioisotopes, the identity of the emitter can be determined. This technique has many applications, particularly in situations where rapid nondestructive analysis is required.

### 1.15.2 Background principles

#### 1.15.2.1 Radioactive decay

The field of chemistry typically concerns itself with the behavior and interactions of stable isotopes of the elements. However, elements can exist in numerous states which are not stable. For example, a nucleus can have too many neutrons for the number of protons it has or contrarily, it can have too few neutrons for the number of protons it has. Alternatively, the nuclei can exist in an excited state, wherein a nucleon is present in an energy state that is higher than the ground state. In all of these cases, the unstable state is at a higher energy state and the nucleus must undergo some kind of decay process to reduce that energy.

There are many types of radioactive decay, but type most relevant to gamma-ray spectroscopy is gamma decay. When a nucleus undergoes radioactive decay by  $\alpha$  or  $\beta$  decay, the resultant nucleus produced by this process, often called the daughter nucleus, is frequently in an excited state. Similar to how electrons are found in discrete energy levels around a nucleus, nucleons are found in discrete energy levels within the nucleus. In  $\gamma$  decay, the excited nucleon decays to a lower energy state and the energy difference is emitted as a quantized photon. Because nuclear energy levels are discrete, the transitions between energy levels are fixed for a given transition. The photon emitted from a nuclear transition is known as a  $\gamma$ -ray.

#### 1.15.2.2 Radioactive decay kinetics and equilibria

Radioactive decay, with few exceptions, is independent of the physical conditions surrounding the radioisotope. As a result, the probability of decay at any given instant is constant for any given nucleus of that particular radioisotope. We can use calculus to see how the number of parent nuclei present varies with time. The time constant,  $\lambda$ , is a representation of the rate of decay for a given nuclei, (1.87).

$$\frac{dN}{N} = -\lambda dt \quad (1.87)$$

If the symbol  $N_0$  is used to represent the number of radioactive nuclei present at  $t = 0$ , then the following equation describes the number of nuclei present at some given time.

$$N = N_0 e^{-\lambda t} \quad (1.88)$$

<sup>33</sup>This content is available online at <<http://cnx.org/content/m38345/1.1/>>.

The same equation can be applied to the measurement of radiation with some sort of detector. The count rate will decrease from some initial count rate in the same manner that the number of nuclei will decrease from some initial number of nuclei.

The decay rate can also be represented in a way that is more easily understood. The equation describing half-life ( $t_{1/2}$ ) is shown in (1.89).

$$t_{1/2} = \frac{\ln 2}{\lambda} \quad (1.89)$$

The half-life has units of time and is a measure of how long it takes for the number of radioactive nuclei in a given sample to decrease to half of the initial quantity. It provides a conceptually easy way to compare the decay rates of two radioisotopes. If one has the same number of starting nuclei for two radioisotopes, one with a short half-life and one with a long half-life, then the count rate will be higher for the radioisotope with the short half-life, as many more decay events must happen per unit time in order for the half-life to be shorter.

When a radioisotope decays, the daughter product can also be radioactive. Depending upon the relative half-lives of the parent and daughter, several situations can arise: no equilibrium, a transient equilibrium, or a secular equilibrium. This module will not discuss the former two possibilities, as they are off less relevance to this particular discussion.

Secular equilibrium takes place when the half-life of the parent is much longer than the half-life of the daughter. In any arbitrary equilibrium, the ratio of atoms of each can be described as in (1.90).

$$\frac{N_P}{N_D} = \frac{\lambda_D - \lambda_P}{\lambda_P} \quad (1.90)$$

Because the half-life of the parent is much, much greater than the daughter, as the parent decays, the observed amount of activity changes very little.

$$\frac{N_P}{N_D} = \frac{\lambda_D}{\lambda_P} \quad (1.91)$$

This can be rearranged to show that the activity of the daughter should equal the activity of the parent.

$$A_P = A_D \quad (1.92)$$

Once this point is reached, the parent and the daughter are now in secular equilibrium with one another and the ratio of their activities should be fixed. One particularly useful application of this concept, to be discussed in more detail later, is in the analysis of the refinement level of long-lived radioisotopes that are relevant to trafficking.

## 1.15.3 Detectors

### 1.15.3.1 Scintillation detector

A scintillation detector is one of several possible methods for detecting ionizing radiation. Scintillation is the process by which some material, be it a solid, liquid, or gas, emits light in response to incident ionizing radiation. In practice, this is used in the form of a single crystal of sodium iodide that is doped with a small amount of thallium, referred to as NaI(Tl). This crystal is coupled to a photomultiplier tube which converts the small flash of light into an electrical signal through the photoelectric effect. This electrical signal can then be detected by a computer.

### 1.15.3.2 Semiconductor detector

A semiconductor accomplishes the same effect as a scintillation detector, conversion of gamma radiation into electrical pulses, except through a different route. In a semiconductor, there is a small energy gap between

the valence band of electrons and the conduction band. When a semiconductor is hit with gamma-rays, the energy imparted by the gamma-ray is enough to promote electrons to the conduction band. This change in conductivity can be detected and a signal can be generated correspondingly. Germanium crystals doped with lithium, Ge(Li), and high-purity germanium (HPGe) detectors are among the most common types.

### 1.15.3.3 Advantages and disadvantages

Each detector type has its own advantages and disadvantages. The NaI(Tl) detectors are generally inferior to Ge(Li) or HPGe detectors in many respects, but are superior to Ge(Li) or HPGe detectors in cost, ease of use, and durability. Germanium-based detectors generally have much higher resolution than NaI(Tl) detectors. Many small photopeaks are completely undetectable on NaI(Tl) detectors that are plainly visible on germanium detectors. However, Ge(Li) detectors must be kept at cryogenic temperatures for the entirety of their lifetime or else they rapidly become incapable of functioning as a gamma-ray detector. Sodium iodide detectors are much more portable and can even potentially be used in the field because they do not require cryogenic temperatures so long as the photopeak that is being investigated can be resolved from the surrounding peaks.

### 1.15.3.4 Gamma spectrum features

There are several dominant features that can be observed in a gamma spectrum. The dominant feature that will be seen is the photopeak. The photopeak is the peak that is generated when a gamma-ray is totally absorbed by the detector. Higher density detectors and larger detector sizes increase the probability of the gamma-ray being absorbed.

The second major feature that will be observed is that of the Compton edge and distribution. The Compton edge arises due to Compton Effect, wherein a portion of the energy of the gamma-ray is transferred to the semiconductor detector or the scintillator. This occurs when the relatively high energy gamma ray strikes a relatively low energy electron. There is a relatively sharp edge to the Compton edge that corresponds to the maximum amount of energy that can be transferred to the electron via this type of scattering. The broad peak lower in energy than the Compton edge is the Compton distribution and corresponds to the energies that result from a variety of scattering angles. A feature in Compton distribution is the backscatter peak. This peak is a result of the same effect but corresponds to the minimum energy amount of energy transferred. The sum of the energies of the Compton edge and the backscatter peak should yield the energy of the photopeak.

Another group of features in a gamma spectrum are the peaks that are associated with pair production. Pair production is the process by which a gamma ray of sufficiently high energy ( $>1.022$  MeV) can produce an electron-positron pair. The electron and positron can annihilate and produce two 0.511 MeV gamma photons. If all three gamma rays, the original with its energy reduced by 1.022 MeV and the two annihilation gamma rays, are detected simultaneously, then a full energy peak is observed. If one of the annihilation gamma rays is not absorbed by the detector, then a peak that is equal to the full energy less 0.511 MeV is observed. This is known as an escape peak. If both annihilation gamma rays escape, then a full energy peak less 1.022 MeV is observed. This is known as a double escape peak.

## 1.15.4 Example of experiments

### 1.15.4.1 Determination of depleted uranium

Natural uranium is composed mostly of  $^{238}\text{U}$  with low levels of  $^{235}\text{U}$  and  $^{234}\text{U}$ . In the process of making enriched uranium, uranium with a higher level of  $^{235}\text{U}$ , depleted uranium is produced. Depleted uranium is used in many applications particularly for its high density. Unfortunately, uranium is toxic and is a potential health hazard and is sometimes found in trafficked radioactive materials, so it is important to have a methodology for detection and analysis of it.

One easy method for this determination is achieved by examining the spectrum of the sample and comparing it qualitatively to the spectrum of a sample that is known to be natural uranium. This type of

qualitative approach is not suitable for issues that are of concern to national security. Fortunately, the same approach can be used in a quantitative fashion by examining the ratios of various gamma-ray photopeaks.

The concept of a radioactive decay chain is important in this determination. In the case of  $^{238}\text{U}$ , it decays over many steps to  $^{206}\text{Pb}$ . In the process, it goes through  $^{234\text{m}}\text{Pa}$ ,  $^{234}\text{Pa}$ , and  $^{234}\text{Th}$ . These three isotopes have detectable gamma emissions that are capable of being used quantitatively. As can be seen in Table 1.13, the half-life of these three emitters is much less than the half-life of  $^{238}\text{U}$ . As a result, these should exist in secular equilibrium with  $^{238}\text{U}$ . Given this, the ratio of activity of  $^{238}\text{U}$  to each daughter products should be 1:1. They can thus be used as a surrogate for measuring  $^{238}\text{U}$  decay directly via gamma spectroscopy. The total activity of the  $^{238}\text{U}$  can be determined by (1.93), where  $A$  is the total activity of  $^{238}\text{U}$ ,  $R$  is the count rate of the given daughter isotope, and  $B$  is the probability of decay via that mode. The count rate may need to be corrected for self-absorption of the sample is particularly thick. It may also need to be corrected for detector efficiency if the instrument does not have some sort of internal calibration.

$$A = R/B \quad (1.93)$$

| Isotope                   | Half-life               |
|---------------------------|-------------------------|
| $^{238}\text{U}$          | $4.5 \times 10^9$ years |
| $^{234}\text{Th}$         | 24.1 days               |
| $^{234\text{m}}\text{Pa}$ | 1.17 minutes            |

**Table 1.13:** Half-lives of pertinent radioisotopes in the  $^{238}\text{U}$  decay chain

**Exercise 1.15.1**

*(Solution on p. 122.)*

A gamma spectrum of a sample is obtained. The 63.29 keV photopeak associated with  $^{234}\text{Th}$  was found to have a count rate of 5.980 kBq. What is the total activity of  $^{238}\text{U}$  present in the sample?

The count rate of  $^{235}\text{U}$  can be observed directly with gamma spectroscopy. This can be converted, as was done in the case of  $^{238}\text{U}$  above, to the total activity of  $^{235}\text{U}$  present in the sample. Given that the natural abundances of  $^{238}\text{U}$  and  $^{235}\text{U}$  are known, the ratio of the expected activity of  $^{238}\text{U}$  to  $^{235}\text{U}$  can be calculated to be 21.72 : 1. If the calculated ratio of disintegration rates varies significantly from this expected value, then the sample can be determined to be depleted or enriched.

**Exercise 1.15.2**

*(Solution on p. 122.)*

As shown above, the activity of  $^{238}\text{U}$  in a sample was calculated to be 123.6 kBq. If the gamma spectrum of this sample shows a count rate 23.73 kBq at the 185.72 keV photopeak for  $^{235}\text{U}$ , can this sample be considered enriched uranium? The emission probability for this photopeak is 57.2%.

This type of calculation is not unique to  $^{238}\text{U}$ . It can be used in any circumstance where the ratio of two isotopes needs to be compared so long as the isotope itself or a daughter product it is in secular equilibrium with has a usable gamma-ray photopeak.

#### 1.15.4.2 Determination of the age of highly-enriched uranium

Particularly in the investigation of trafficked radioactive materials, particularly fissile materials, it is of interest to determine how long it has been since the sample was enriched. This can help provide an idea of the source of the fissile material—if it was enriched for the purpose of trade or if it was from cold war era enrichment, etc.

When uranium is enriched,  $^{235}\text{U}$  is concentrated in the enriched sample by removing it from natural uranium. This process will separate the uranium from its daughter products that it was in secular equilibrium with. In addition, when  $^{235}\text{U}$  is concentrated in the sample,  $^{234}\text{U}$  is also concentrated due to the particulars of the enrichment process. The  $^{234}\text{U}$  that ends up in the enriched sample will decay through

several intermediates to  $^{214}\text{Bi}$ . By comparing the activities of  $^{234}\text{U}$  and  $^{214}\text{Bi}$  or  $^{226}\text{Ra}$ , the age of the sample can be determined.

$$A_{\text{Bi}} = A_{\text{Ra}} = \frac{A_{\text{U}}}{2} \lambda_{\text{Th}} \lambda_{\text{Ra}} T^2 \quad (1.94)$$

In (1.94),  $A_{\text{Bi}}$  is the activity of  $^{214}\text{Bi}$ ,  $A_{\text{Ra}}$  is the activity of  $^{226}\text{Ra}$ ,  $A_{\text{U}}$  is the activity of  $^{234}\text{U}$ ,  $\lambda_{\text{Th}}$  is the decay constant for  $^{230}\text{Th}$ ,  $\lambda_{\text{Ra}}$  is the decay constant for  $^{226}\text{Ra}$ , and  $T$  is the age of the sample. This is a simplified form of a more complicated equation that holds true over all practical sample ages (on the order of years) due to the very long half-lives of the isotopes in question. The results of this can be graphically plotted as they are in .

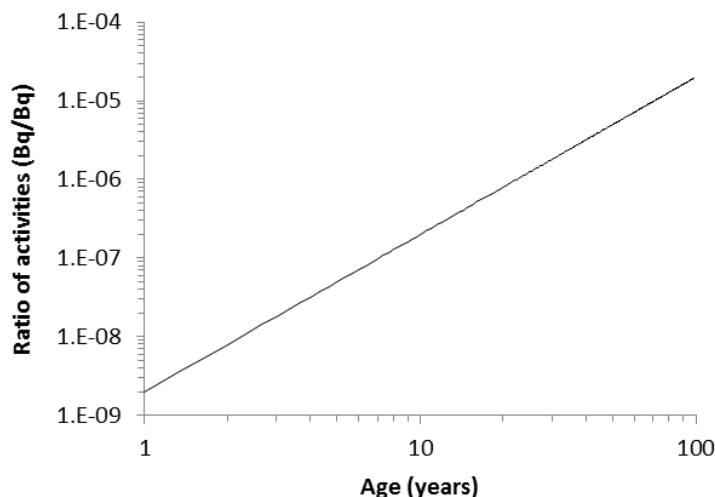


**Figure 1.100:** Ratio of  $^{226}\text{Ra}/^{234}\text{U}$  ( $= ^{214}\text{Bi}/^{234}\text{U}$ ) plotted versus age based on (1.94). This can be used to determine how long ago a sample was enriched based on the activities of  $^{234}\text{U}$  and  $^{226}\text{Ra}$  or  $^{214}\text{Bi}$  in the sample.

### Exercise 1.15.3

(Solution on p. 123.)

*Exercise:* The gamma spectrum for a sample is obtained. The count rate of the 121 keV  $^{234}\text{U}$  photopeak is 4500 counts per second and the associated emission probability is 0.0342%. The count rate of the 609.3 keV  $^{214}\text{Bi}$  photopeak is 5.83 counts per second and the emission probability is 46.1%. How old is the sample?

### 1.15.5 References

- G. Choppin, J.-O. Liljenzin, and J. Rydberg. *Radiochemistry and Nuclear Chemistry*, Elsevier Press, Oxford (2006).
- W. Loveland, D. J. Morrissey, and G. T. Seaborg. *Modern Nuclear Chemistry*, Wiley, New Jersey (2006).
- K. Mayer, M. Wallenius, and I. Ray. *Analyst*, 2005, **130**, 433.

- J. T. Mihalczo, J. A. Mullens, J. K. Mattingly, and T. E. Valentine. *Nucl. Instrum. Meth. A*, 2000, **450**, 531.
- J. T. Mihalczo, J. K. Mattingly, J. S. Neal, and J. A. Mullens, *Nucl. Instrum. Meth. B*, 2004, **213**, 378.
- K. J. Moody, I. A. Hutcheon, and P. M. Grant. *Nuclear Forensic Analysis*, CRC Press, Boca Raton (2005).
- C. T. Nguyen. *Nucl. Instrum. Meth. B*, 2005, **229**, 103.
- C. T. Nguyen, and J. Zsigrai. *Nucl. Instrum. Meth. B*, 2006, **246**, 417.
- D. Reilly, N. Ensslin, and H. Smith, Jr. *Passive Nondestructive Assay of Nuclear Materials*, National Technical Information Service, Springfield, VA (1991).
- M. Wallenius, A. Morgenstern, C. Apostolidis, and K. Mayer. *Anal. Bioanal. Chem.*, 2002, **374**, 379.

## Solutions to Exercises in Chapter 1

### Solution to Exercise 1.3.1 (p. 13)

The fuel mole fraction is 4.03%.

### Solution to Exercise 1.3.2 (p. 16)

The empirical formula is  $C_3H_7$ , and the molecular formula is  $(C_3H_7)_6$  or  $C_{18}H_{42}$ .

### Solution to Exercise 1.3.3 (p. 18)

The empirical formula is  $C_4H_8O$ , and the molecular formula is  $(C_4H_8O)_2$  or  $C_8H_{16}O_2$ . Possible compounds with this molecular formula are shown in (Figure 1.101).

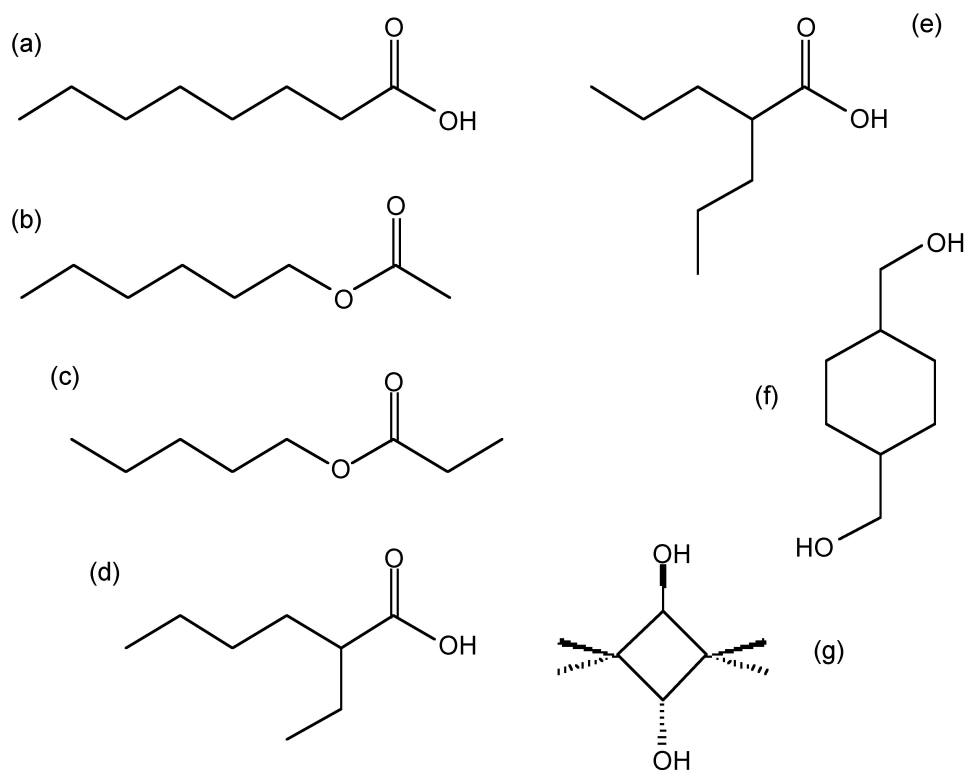


**Figure 1.101:** Structure of possible compounds with the molecular formula  $C_8H_{16}O_2$ : (a) octanoic acid (caprylic acid), (b) hexyl acetate, (c) pentyl propanoate, (d) 2-ethyl hexanoic acid, (e) valproic acid (VPA), (f) cyclohexanedimethanol (CHDM), and (g) 2,2,4,4-tetramethyl-1,3-cyclobutandiol (CBDO).

### Solution to Exercise 1.3.4 (p. 19)

The chemical formula is  $Cu_2O$ , and Cu has a 1+ oxidation state.

### Solution to Exercise 1.15.1 (p. 119)

$^{234}Th$  exists in secular equilibrium with  $^{238}U$ . The total activity of  $^{234}Th$  must be equal to the activity of the  $^{238}U$ . First, the observed activity must be converted to the total activity using Equation  $A=R/B$ . It is known that the emission probability for the 63.29 keV gamma-ray for  $^{234}Th$  is 4.84%. Therefore, the total activity of  $^{238}U$  in the sample is 123.6 kBq.

### Solution to Exercise 1.15.2 (p. 119)

As shown in the example above, the count rate can be converted to a total activity for  $^{235}U$ . This yields a total activity of 41.49 kBq for  $^{235}U$ . The ratio of activities of  $^{238}U$  and  $^{235}U$  can be calculated to be 2.979.

This is lower than the expected ratio of 21.72, indicating that the  $^{235}\text{U}$  content of the sample greater than the natural abundance of  $^{235}\text{U}$ .

**Solution to Exercise 1.15.3 (p. 120)**

*Solution:* The observed count rates can be converted to the total activities for each radionuclide. Doing so yields a total activity for  $^{234}\text{U}$  of 4386 kBq and a total activity for  $^{214}\text{Bi}$  of 12.65 Bq. This gives a ratio of  $9.614 \times 10^{-7}$ . Using , as graphed this indicates that the sample must have been enriched 22.0 years prior to analysis.

